DOKUZ EYLÜL UNIVERSITY

GRADUATE SCHOOL OF NATURAL AND APPLIED SCIENCES

INVESTIGATION OF SOIL-PILE-SOIL INTERACTION FOR ORTHOGONAL BARRETTE PILES

by

Yaşar TANER

June, 2022

İZMİR

INVESTIGATION OF SOIL-PILE-SOIL INTERACTION FOR ORTHOGONAL BARRETTE PILES

A Thesis Submitted to the

Graduate School of Natural and Applied Sciences of Dokuz Eylül University

In Partial Fulfillment of the Requirements for Master of Degree in Civil Engineering, Geotechnical Engineering Program

by

Yaşar TANER

June, 2022

İZMİR

M.Sc THESIS EXAMINATION RESULT FORM

We have read the thesis entitled ‘‘**INVESTIGATION OF SOIL-PILE-SOIL INTERACTION FOR ORTHOGONAL BARRETTE PILES**’’ completed by **YAŞAR TANER** under supervision of **PROF. DR. GÜRKAN ÖZDEN** and we certify that in our opinion it is fully adequate, in scope and quality, as a thesis for the degree of Master of Science.

Prof. Dr. Gürkan ÖZDEN

Supervisor

Prof. Dr. Yeliz YÜKSELEN AKSOY

(Jury Member)

Asst. Prof. Dr. M. Rıfat KAHYAOĞLU

(Jury Member)

Prof. Dr. Okan FISTIKOĞLU

Director

Graduate School of Natural and Applied Sciences

ACKNOWLEDGEMENTS

First and foremost, I am extremely grateful to my supervisor, Prof. Dr. Gürkan Özden, for his invaluable advice, continuous support, and patience during my MSc study. Their immense knowledge and great experience have encouraged me in my academic research and daily life. I would like to thank all the members of the Geotechnical Engineering Division of Civil Engineering of Dokuz Eylul University. Finally, I would like to express my gratitude to my parents, wife, and sister. Without their tremendous understanding and encouragement in the past few years, it would be impossible to complete my study.

Yaşar TANER

INVESTIGATION OF SOIL-PILE-SOIL INTERACTION FOR ORTHOGONAL BARRETTE PILES

ABSTRACT

In recent years, tall building design and construction accelerated in Turkey. Barrette piles have been preferred over circular bored piles due to their higher load-bearing capacity and bending stiffness to carry induced loads by the superstructure.

In this thesis, four different cohesionless soils with different relative densities and different pile spacings were modeled in order to investigate the pile groups under lateral loads. Barrette piles were modeled as volumetric elements in order to examine shape effects more accurately. In this context, the effects of the cross-section and orientation of the piles in the group, spacing between the piles, the soil stiffness and the magnitude of loading on the behavior of the group barrette piles were investigated under linear and nonlinear soil conditions. Considering these effects, the horizontally loaded barrette pile groups were analyzed in the finite element program and the interaction factors between the piles were calculated. Since the cross-sections of the barette piles are rectangular, the most important factor in their interaction with each other was the bending stiffness of the pile in the direction of the load acting on the pile. Analysis results revealed that the interaction between barrette piles is quite different from that of circular piles, mostly depending on the type of pile cross section. In addition, it was concluded that the shading effect is quite effective for both free and fixed head pile groups.

Keywords: Lateral loaded piles, interaction factor, barrette pile, pile orientation, pile-soil-pile interaction.

ORTOGONAL BARET KAZIKLAR İÇİN ZEMİN-KAZIK-ZEMİN ETKİLEŞİMİNİN İNCELENMESİ

ÖZ

Son yıllarda Türkiye'de yüksek bina tasarımı ve yapımı hız kazandı. Baret kazıklar, üst yapının zemine aktardığı yükleri taşımak için daha yüksek yük taşıma kapasiteleri ve eğilme rijitliklerine sahip olduklarından dairesel fore kazıklara göre daha çok tercih edilmektedir.

Bu tezde yatay yükler altındaki baret kazık gruplarını araştırabilmek için, relative sıkılıkları farklı olan dört farklı kohezyonsuz zemin ve farklı kazık aralıkları ile model kurulmuştur. Baret kazıklar, şekil etkilerini daha doğru bir şekilde inceleyebilmek için hacimsel eleman olarak modellenmiştir. Bu bağlamda kazıkların kesit ve grup içindeki yerleşimleri, kazıklar arası mesafe, zemin rijitliği ve yükleme büyüklüğünün grup baret kazıkların davranışı üzerindeki etkileri linear ve nonlinear zemin koşulları altında araştırılmıştır. Bu etkiler göz önünde bulundurularak yatay yüklü baret kazık grupları sonlu elemanlar programında analiz edilerek kazıklar arasında etkileşim faktörleri hesaplanmıştır. Baret kazıkların enine kesitleri dikdörtgen olduğundan, birbirleriyle etkileşimlerinde en önemli faktör, yükün kazık üzerine etkidiği yöndeki kazığın eğilme rijitliği belirleyici olmuştur. Analiz sonuçları, baret kazıklar arasındaki etkileşimin, en çok kazık kesitinin tipine bağlı olarak dairesel kazıklardan oldukça farklı olduğunu ortaya koymuştur. Ayrıca gölgeleme etkisi hem serbest hem de sabit başlı kazık grupları için oldukça etkili olduğu sonucuna varılmıştır.

Anahtar kelimeler: Yanal yüklü kazıklar, etkileşim faktörü, baret kazık, kazık yerleşimi, kazık-zemin-kazık etkileşimi.

CONTENTS

LIST OF FIGURES

Page

LIST OF TABLES

CHAPTER ONE
INTRODUCTION

1.1 Introduction

The performance-based design of pile foundations needs a rational understanding of interaction mechanisms between pile-soil and pile-soil-pile inside foundations of structures (Bradley et al., 2008; Kramer et al., 2014; Rotta Loria, 2018). Foundations that transfer structural loads to deeper soil layers are rarely designed with single piles. The interaction between a single pile and surrounding soil is relatively simpler than pile groups since complex interaction patterns exist among the piles and the soil inside a group.

Pile-soil-pile interaction has long been studied since sixties. The pioneering work is attributed to Harry Poulos, who studied interaction among group piles under vertical and lateral loads (Poulos, 1968, 1979; Poulos & Davis, 1980). Following Poulos, contributions to the field were also made (Banerjee & Davies, 1980; Brown et al., 1988). Kaynia and Kausel (Kaynia & Kausel, 1980) extended Poulos' approach to dynamic loading conditions.

The scarcity of building parcels in urban areas triggered the construction of high-rise buildings, especially in coastal regions. Such buildings are designed with piles that are much deeper with larger sections. In this respect, barrette piles are usually preferred over circular piles since they provide larger bearing capacity, stiffness, and structural capacity.

Previous research did not cover pile-soil-pile interaction among piles with rectangular sections. Currently, design work with such piles is usually made assuming an equivalent circular pile diameter. In this study, findings of finite element-based research are presented regarding the influence of loading direction, pile spacing, the position of a pile in the group, and soil nonlinearity on interaction factors produced for barrette piles. The three-dimensional nature of the problem necessitated the establishment of 3D numerical analysis models. Piles are modeled as volume elements to study shape and shadowing effects properly.

CHAPTER TWO
THE STATEMENT OF THE PROBLEM

2.1 Problem and Hypothesis

In recent times, extensive theoretical approaches have been developed for predicting the soil-pile-soil interaction on laterally loaded circular piles. Many researchers (Poulos & Davis, 1980; Mylonakis & Gazetas, 1998; Randolph & Wroth, 1979) have presented several methods, curves, and tables for reference. However, previous research did not cover pile-soil-pile interaction among piles with rectangular sections under horizontal loads.

Despite their widespread usage, the interaction of barrette piles with surrounding soil during earthquake loading is still analyzed using conventional load-deformation curves that were developed for circular piles.

It is thought that modeling barrette piles subjected to horizontal loads as equivalent circular piles are not an appropriate approach, especially under horizontal loads due to pile orientation, soil nonlinearity, pile head fixity, and pile spacing.

In this study, it is aimed to reveal the different behavior of barrette piles under horizontal loads with finite element-based analyses related to the loading direction, pile spacing, position of the piles within the group, and the effect of soil nonlinearity on the interaction factors produced for barrette piles.

2.2 Methodology

2.2.1 Calculation of Interaction Factors

In Poulos' theory, two identical, equally loaded circular piles are considered, each pile being divided into a number of elements, as for the single pile shown in Figure 2.1 and he calculated the interaction factors by assuming that the horizontal displacements of the soil and the displacements of each element on the pile will be equal while the elastic conditions prevail within the soil.

Poulos' theory is based on some assumptions. First of all, the pile is assumed to be a thin rectangular vertical strip of width d, length L with a constant flexibility E_pI_p. It is also assumed that the pile and soil are fully compatible, ignoring the relative motion of the pile and soil. The soil is assumed to be elastic. Mindlins' equation regarding the horizontal displacements as a result of point load action inside the soil is integrated along pile depth to obtain pile displacements and interaction factors. The side shear, which is expected to be quite influential on lateral pile response for rectangular cross-sections, is not accounted for in Poulos' solution. Interaction factor is defined according to Poulos as in Eq. 2.1:

$$\alpha = \frac{Additional\ displacement\ caused\ by\ adjacent\ pile}{Displacement\ of\ pile\ under\ its\ own\ load} \qquad (2.1)$$

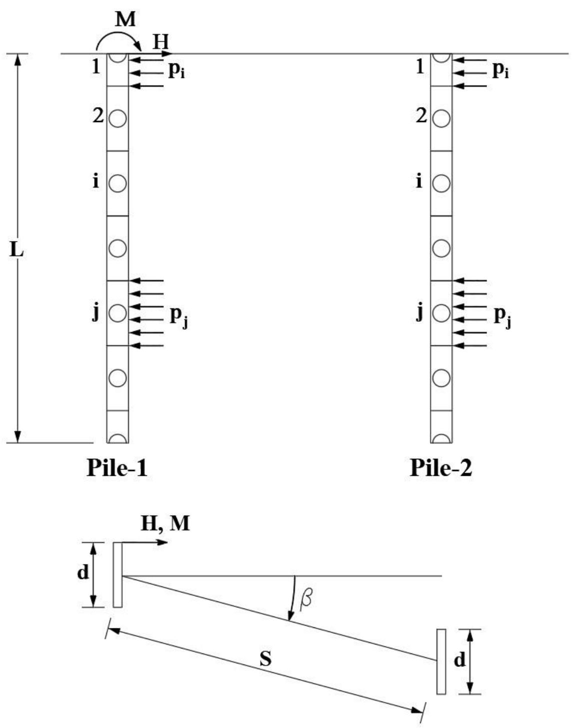

Figure 2.1 Laterally loaded piles (H. G. Poulos, 1968)

The orthogonal distance, s, between any two consecutive piles changes in direct proportion to the plan width of the pile. Soil layers are modeled as linear and nonlinearly behaving materials obeying the rules of the linear and hardening small strain model (PLAXIS3D Material Models, 2021).

2.2.2 Finite Element Method

Even though the lateral soil-pile-soil interaction is three-dimensional (3D), the empirical techniques described above reduce the problem to a two-dimensional (2D) plane strain problem. There are considerable changes between 2D and 3D failure planes, necessitating a thorough examination of the interaction and behavior of soil-pile-soil in barrette piles (Ashour et al., 2001). Because this study aims to investigate laterally loaded piles and pile groups for horizontal loads while taking into account the 3D effect, a 3D FEM (PLAXIS3D) software, is utilized to estimate the soil-pile-soil interaction of orthogonal barrette piles.

The response of the piling groups under horizontal loading is calculated in this thesis using the FEM code PLAXIS 3D and a series of comprehensive numerical calculations. It is a well-known algorithm in geotechnical engineering for stress-strain, stability, and groundwater ow analysis. It was first developed in 1987 at Delft University of Technology, and it has since been expanded to include a wide range of geotechnical engineering topics. In 2001, capability for 3D analysis was added.

PLAXIS 3D includes an entirely 3D graphical processor that enables simple graphical input of complicated geometry models as well as an illustrated display of the results. Most FE meshes are created automatically, utilizing algorithms for mesh regularity checking. Beams, anchors, plates, and geogrids are just a few of the structural components that may be modeled. Staged (phase) analysis is also available, allowing for accurate modeling of the geotechnical design of pile foundations, shoring systems, etc., beginning with the initial stress levels.

The finite element method's basic concept is to find a complicated problem by substituting this with simpler. We will only find an approximate solution rather than an exact one because the genuine problem is replaced by a simpler one in solving the problem. Most real problems will require more existing mathematical methods to provide an accurate answer.

The finite element method can be chosen without any other efficient method to find even an approximate solution to a given problem. Moreover, the finite element approach is generally the way to improve or refine the approximate answer by putting in more computational effort (Rao, 2004).

PLAXIS 3D implements full 3D (solid) pile modeling techniques. Piles are discretized utilizing 3D (solid) finite elements in the full 3D analysis. The fact that the pile geometry and soil-structure interaction are accurately described is an advantage of this kind of modeling. However, due to its computational complexity, this typically results in extensive models, which can be time-consuming in common engineering practice.

PLAXIS 3D software employs 10 noded tetrahedral mesh components to represent soil (Figure 2.2). For structural items and interface components, several mesh elements are employed. A finite element computation relies heavily on mesh formation. Meshes should be fine enough to get accurate results while coarse enough to minimize excessive computation times. This software provides five different ways to generate finite element meshes. Extremely coarse, coarse, medium, fine, and very fine meshes are available. Aside from these basic choices, the fineness factor that is established for all geometric entries may be changed to provide the necessary level of mesh fineness and local refinement for a specific volume or structural item.

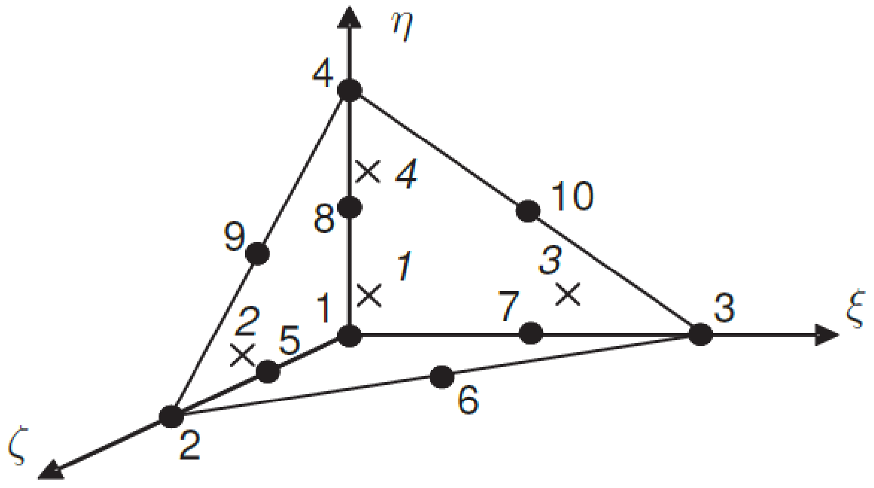

Figure 2.2 10 noded tetrahedral mesh component

2.2.1.1 Linear Elastic Model

The linear elastic model in PLAXIS 3D is based on the generalized Hooke's law of isotropic elasticity. It includes two basic elastic parameters, Young's modulus E and Poisson's ratio. Stress states in the linear elastic model in this FEM software are not limited, meaning the simulated material can have infinite strength. However, to simulate the piles using the linear elastic model, one should ensure that the pile material, such as concrete strength, is not exceeded in the considered problem.

2.2.1.2 Nonlinear Soil Model

The Hardening Soil model is a new adaptation of the non-linear elastic structure model developed for different soft and hard soil by (Duncan&Chang, 1970), describing the stress-strain relationship of the soil as approximately hyperbolic (Schanz et al., 1999). In particular, considering the increase in stiffness due to stress, three different stiffness parameters, loading-unloading, and elastic-plastic separation, enable this body model to model the soil stress-strain behavior closer to reality.

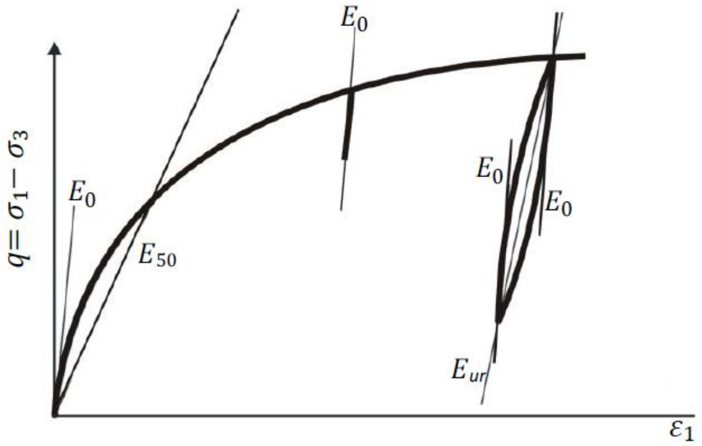

Figure 2.3 Representative stiffness parameters in a triaxial shear test

Stiffness parameters of HSsmall model, power for the stress-level dependency of stiffness (m), reference stress (p_{ref}), and final stress ratio (R_f) parameters from the hyperbolic equation are used. The main features of the model include the change in stiffness due to stress (input parameter m), plastic deformations in primary deviatoric loading (input parameter E_{50}), plastic deformations due to primary compression (input parameter E_{oed}), and elastic unloading/loading (E_{ur}). These parameters are shown in Figure 2.3 and are obtained from triaxial tests (Benz, 2006).

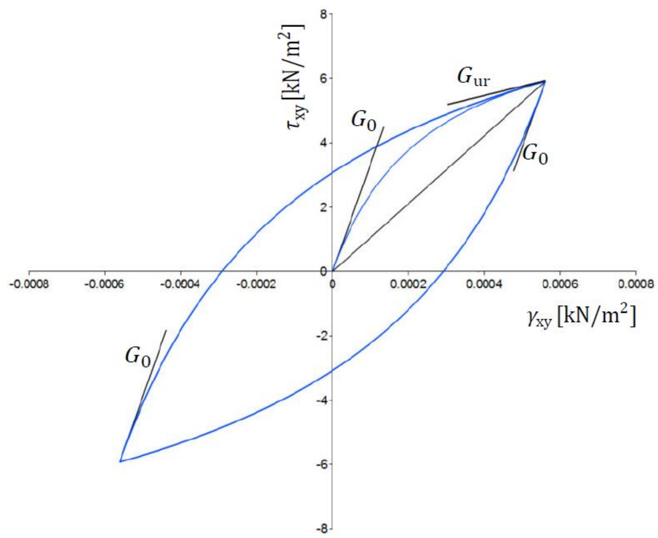

Figure 2.4 Representative stiffness parameters in a cyclic shear test

Two additional stiffness parameters are required as input to the Hardening Soil model with small-strain stiffness: G_0 and $\gamma_{0.7}$. For a reference minor primary stress of pref, G_0 defines the shear modulus at very low strains as shown in Figure 2.4. The Poisson's ratio ν_{ur} is assumed to be constant, therefore, the shear modulus G_0 can be derived using the very low strain Young's modulus as follows:

$$G_0 = \frac{E_0}{2(1+\nu_{ur})} \tag{2.1}$$

CHAPTER THREE
NUMERICAL MODELLING

3.1 Numerical Models

In this thesis, pile groups consisting of 3x3 and 4x4 piles with rectangular cross-sections were subjected to finite element modelling free-head models and fixed head model, respectively. The finite element model comprises three-dimensional 10-noded wedge elements to discretize the volume piles and the soil profile. The aspect ratio of the pile cross-section is set as L/B=3.5, where L and B stand for length and width of the pile section, respectively. This assumption is based on the fact that barrette piles are usually constructed with L=280 cm and B=80 cm sectional dimensions. Only very deep super piles attain plan width that is B≥100 cm. The auto-meshing algorithm of the FE analysis software (PLAXIS 3D) was utilized while establishing the 3D-FEM model. The pile length to diameter ratio was kept equal to $L_{pile}/B=25$ throughout the analyses. A 3D view of the model with solid piles for free-head and fixed-head pile groups are shown in Figure 3.1 and Figure 3.2. It can be seen in this figure that the piles are positioned orthogonal to each other in the model.

3.1.1 3x3 Free-Head Elastic Model

In numerical analysis, two-layer profile was considered for barrette piles where stiff-ness of the upper layer was one half of that of the bottom layer. The thickness of the upper layer (h_1) is 10 m and the total thickness of the soil profile (h) is 40 m. Both soils are assumed to exhibit linear behavior under pile head lateral loading. The elastic soil parameters assigned to the soil layers of the model is shown in Table 3.1.

Table 3.1 Elastic model parameters

E' (MPa)	γ_{unsat} (kN/m^3)	γ_{sat} (kN/m^3)	ν
30	17.0	19.8	0.3/0.5
60	19.0	20.6	0.3/0.5

The edge-to-edge orthogonal distance, s, between any two consecutive piles changes in direct proportion to the plan width of the pile (i.e. s=2B~8B). Each pile is horizontally loaded at the head in both x and y directions. Only very deep super piles attain plan width that is B≥100 cm.

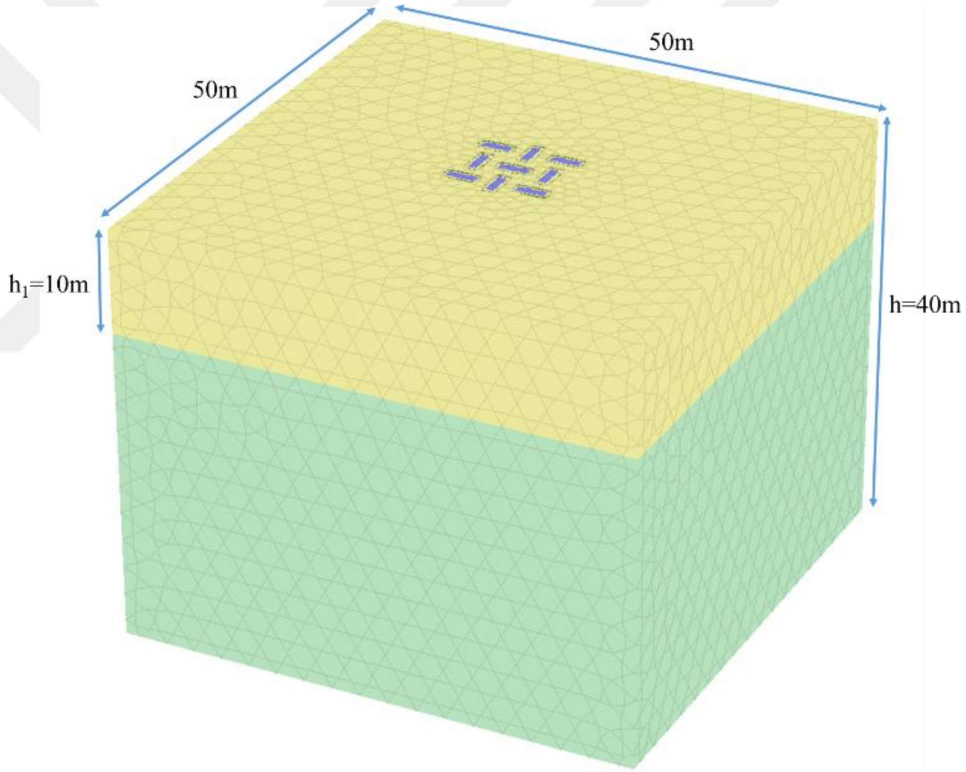

Figure 3.1 FEM mesh for 3x3 barrette pile group (10-noded 31028 elements)

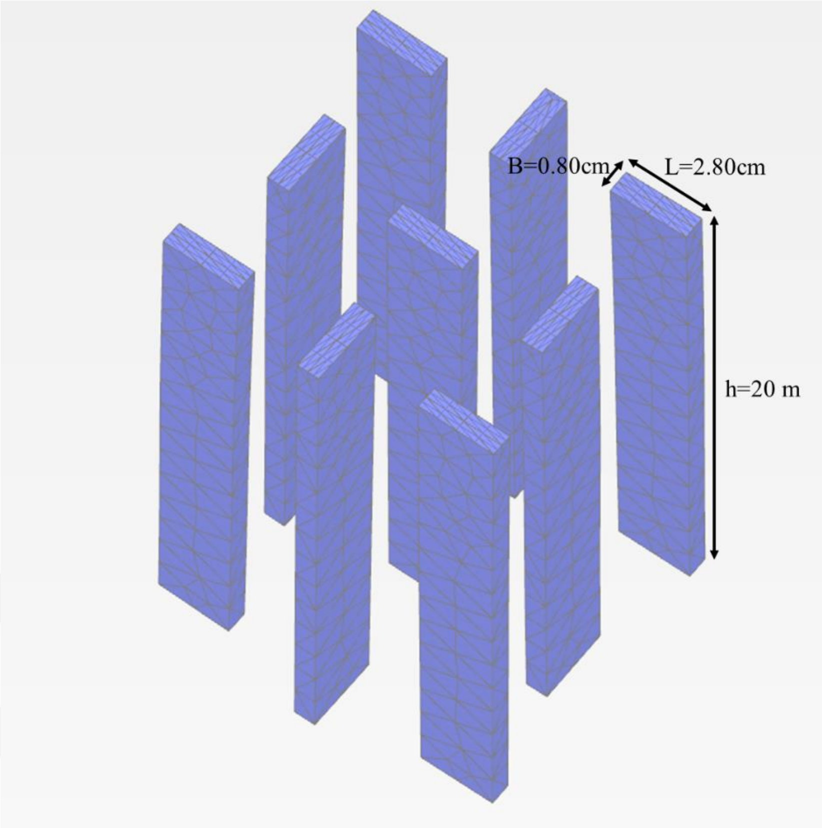

Figure 3.2 Meshing of the volumetric barrette piles

3.1.2 3x3 Free-Head Nonlinear Model

Influence of soil density on barrette pile response was studied considering a two-layer profile for which the stiffness of the upper layer varies with respect to that of the lower one with a ratio of 0.25 (RD= 25%), 0.50 (RD=50%), 0.75 (RD=%80) and 1.0 (RD=100%) as can been in Table 3.1. The thickness of the upper layer (h_1) is arranged such that it is equal to either 0.125h (5m), h (40m) being the total thickness of the soil profile as shown in Figure 3.1. Both soils are assumed to exhibit nonlinear behavior under lateral pile head loading. The HSsmall parameters assigned to the soil layers of the model are based on a study where carefully reviewed cases are provided for a wide range of relative densities. The HSsmall soil parameters assigned to the soil layers of the model is shown in Table 3.2. (Brinkgreve & Engin, 2010)

Table 3.2 Nonlinear soil properties (after Brinkgreve & Engin, 2010)

RD	**γ_{unsat}**	**γ_{sat}**	**E_{50}^{ref}**	**E_{oed}^{ref}**	**E_{ur}^{ref}**
%	kN/m^3	kN/m^3	MPa	MPa	MPa
25	16.0	19.4	15	15	45
50	17.0	19.8	30	30	90
80	18.2	20.3	48	48	144
100	19.0	20.6	60	60	180
G_0^{ref}	**$\gamma_{0.7}$**	**ϕ'**	**ψ**	**m**	**R_f**
MPa	-	°	°	-	-
77	$1.8\cdot10^{-4}$	31.1	1.1	0.622	0.969
94	$1.5\cdot10^{-4}$	34.3	4.3	0.544	0.938
114	$1.2\cdot10^{-4}$	38.0	8.0	0.450	0.900
128	$1.0\cdot10^{-4}$	40.5	10.5	0.388	0.875

The auto-meshing algorithm of the FE analysis software (Plaxis BV., 2016) is utilized while establishing the 3D-FEM model. The quality sphere parameter usually characterizes the quality of tetrahedron elements (PLAXIS3D Material Models, 2021). A check on this parameter reveals that its variation range is between 0.3 and 1.0, where 99% of 31028 elements in the model attain quality sphere values not less than 0.5. Barrette piles are modeled as elastic solid volumetric elements. In this manner, it is considered that three-dimensional effects of the pile cross-section on soil-pile interaction are better taken into consideration. Besides, the solid volumetric elements can still provide pile sectional forces. The pile length to diameter ratio was kept equal to $L_{pile}/B=25$ throughout the entire analyses campaign.

3.1.3 4x4 Fixed-Head Nonlinear Model

In order to analyze the shadowing effect on the barrette pile group, a 4x4 fixed-head barrette pile group was created with a rigid plate serving as the pile cap in the model. The pile group was then laterally loaded by defining a surface traction ranging between 20 and 100 kPa with 20 kPa increments. In order to provide complete pile head fixity between the cap and the piles 10 pieces of rigid embedded beam portions were placed for each pile. The optimum number of such embedded beam elements were decided upon several trials until rotation of the pile heads were avoided. The success of this modeling stage was also checked by comparing the sum of the lateral loads shared by each pile with the total applied load at the cap. A two-layer soil profile was considered for which the relative density of the upper layer was set to one half of the below layer of which density was RD=100%. The assigned parameters to each layer are given in the Table 3.1. The thickness of the upper layer (h_1) was kept constant being equal to 0.25h (i.e. 10 m) where h was 40m total thickness of the soil profile as shown in Figure 3.3. The deflected shape of the 4x4 fixed-head pile group is shown in Figure 3.4 proving that full pile head fixity was achieved.

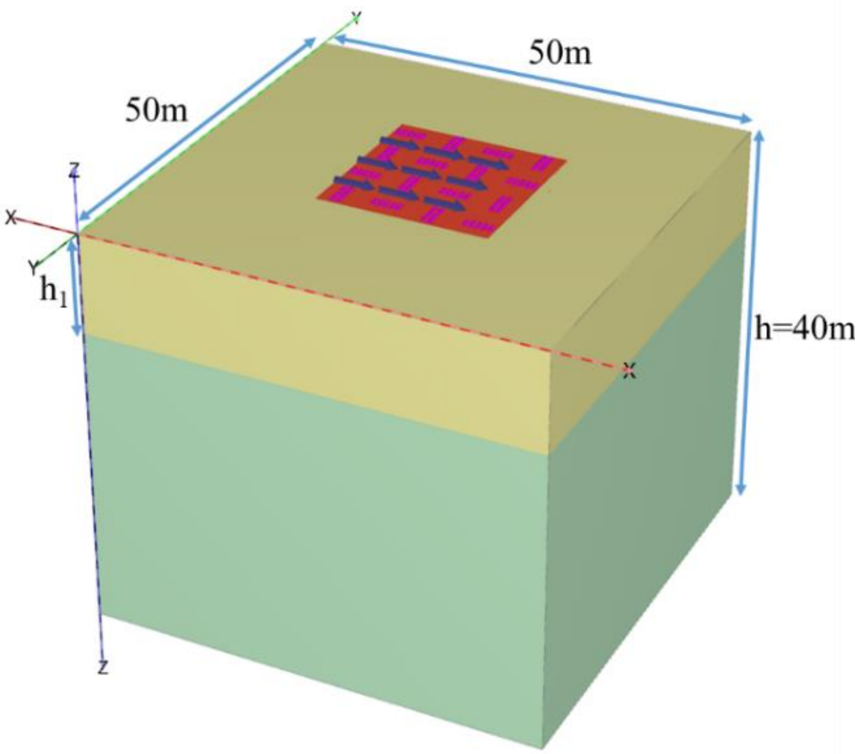

Figure 3.3 4x4 fixed-head barrette group

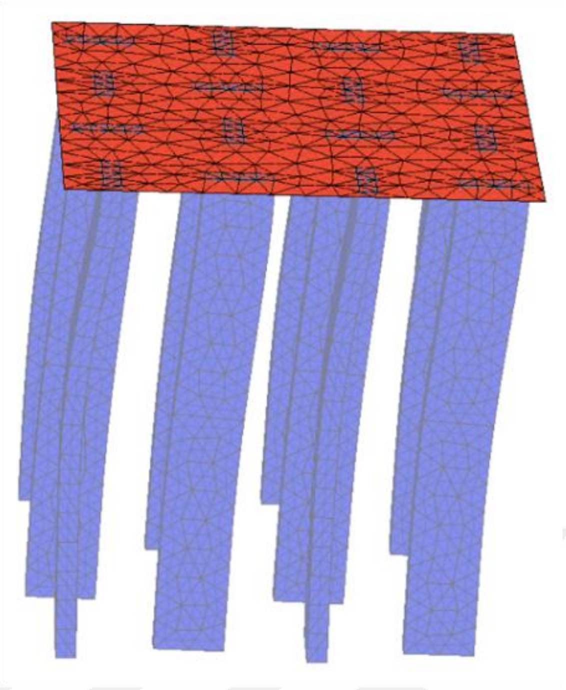

Figure 3.4 Deflected shape of 4x4 fixed-head pile group under x-direction lateral loading

CHAPTER FOUR
RESULTS AND DISCUSSIONS

4.1 3D Numerical Analyses with Linear Elastic Soil Model

The source pile was loaded by means of a distributed lateral load at the pile head with a magnitude of 100 kPa for an 80x280 barrette pile. Interaction factors were determined depending on pile orientation for rectangular cross-sections since loading the piles along their strong or weak axis would generate different effects on adjacent piles. In Case-1 and Case-2, the source piles interact with each neighboring pile, and the amount of interaction varies depending on the position of each receiver pile, as shown in Figure 4.1. The source and receiver piles in similar positions with respect to the loading direction are linked to the source pile with the same color.

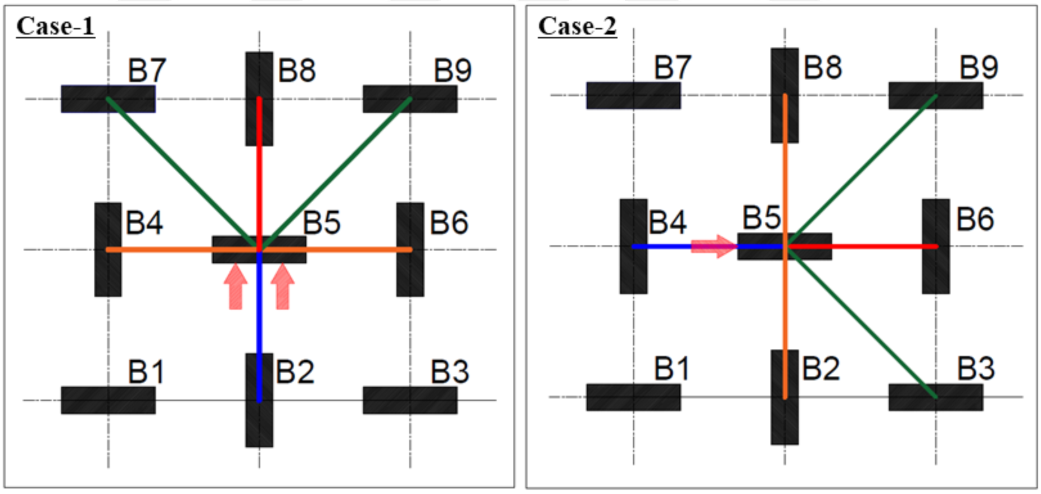

Figure 4.1. Case-1 (loading along minor pile axis), and Case-2 (loading along major pile axis)

Analyses revealed that the location and orientation of the receiver pile with respect to the source played an essential role on the lateral interaction factors. It was found that whether the strong axis of the receiver pile was parallel or perpendicular to the loading direction made the largest difference in pile response. While investigating the influence of pile position, it was noticed that the piles behind and in front of the receiver yielded same interaction factors irrespective of the pile spacing. Similar response existed for other pile pairs (i.e. B4&B6; B7&B9). This behavior may be attributed to the elastic nature of the soil medium and full bonding assumed between the soil and the pile.

Poisson's ratio affected pile response, albeit minor, causing larger lateral deformations resulting in larger interaction factors at the edge piles of the group. Interaction factors are plotted as a function of pile spacing and Poisson's ratio in Figures 4.2 and 4.3 for Case-1 and Case-2, respectively. Figures 4.2 and 4.3 show that the piles are clustered as leading-trailing and side piles with respect to the central one (B5) on which the load is applied. It may be concluded upon elastic analyses that the orientation of the source pile or the piles positioned around the source is the dominant factor. For instance, if the source pile is loaded along its strong axis, its displacement decreases as compared with other direction resulting in higher interaction factors as shown in Figure 4.3. This is also true for the receiver piles indicating that the bending stiffness governs pile response.

The interaction factors computed for 3x3 circular and barrette pile groups are compared in Figures 4.4 and 4.5. It should be mentioned that the edge-to-edge spacing between two piles in a group is the same for both cases. It has been stated above that the interaction between the barrette piles varies according to the position of the pile just in front of the loaded pile. In this analyss, it was found that in the analyses made with circular piles that have a sectional area equivalent to those of the barrettes, loading direction did not affect the interaction between the circular piles since they have the same inertia in all directions. It is clear from Figures 4.4 and 4.5 that Case-1, in which the receiver pile was loaded along the weak axis, yielded lower interaction factors.

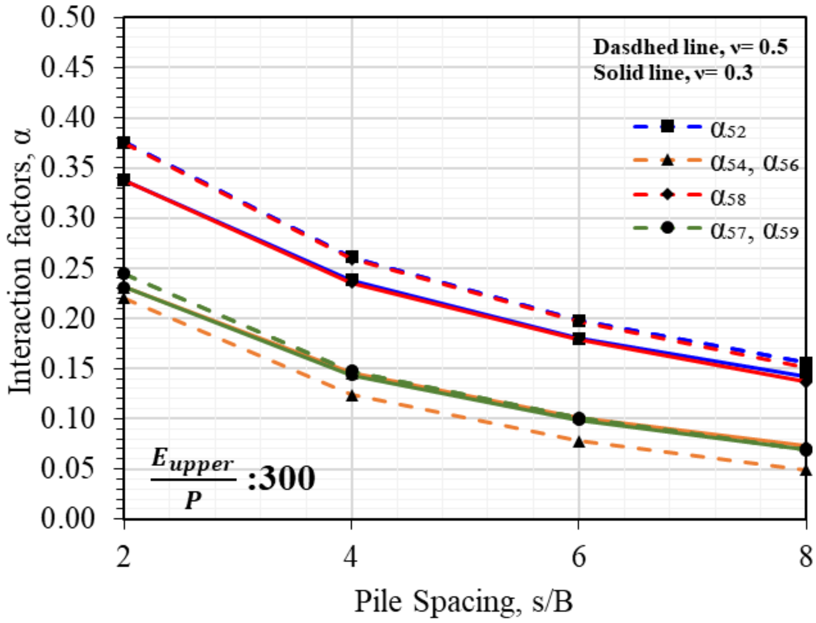

Figure 4.2 Interaction factors between source pile B5 and receiver piles with different Poisson ratio in Case-1

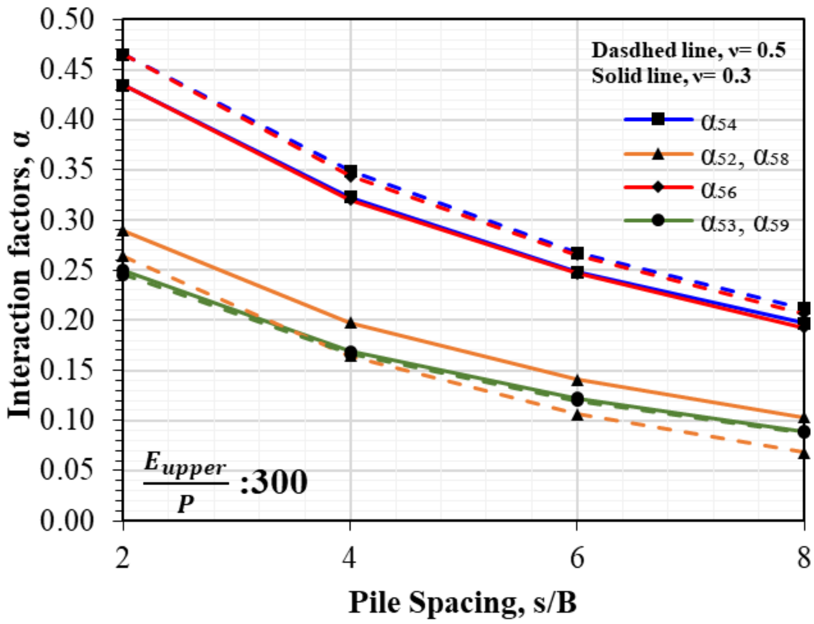

Figure 4.3 Interaction factors between source pile B5 and receiver piles with different Poisson ratio in Case-2

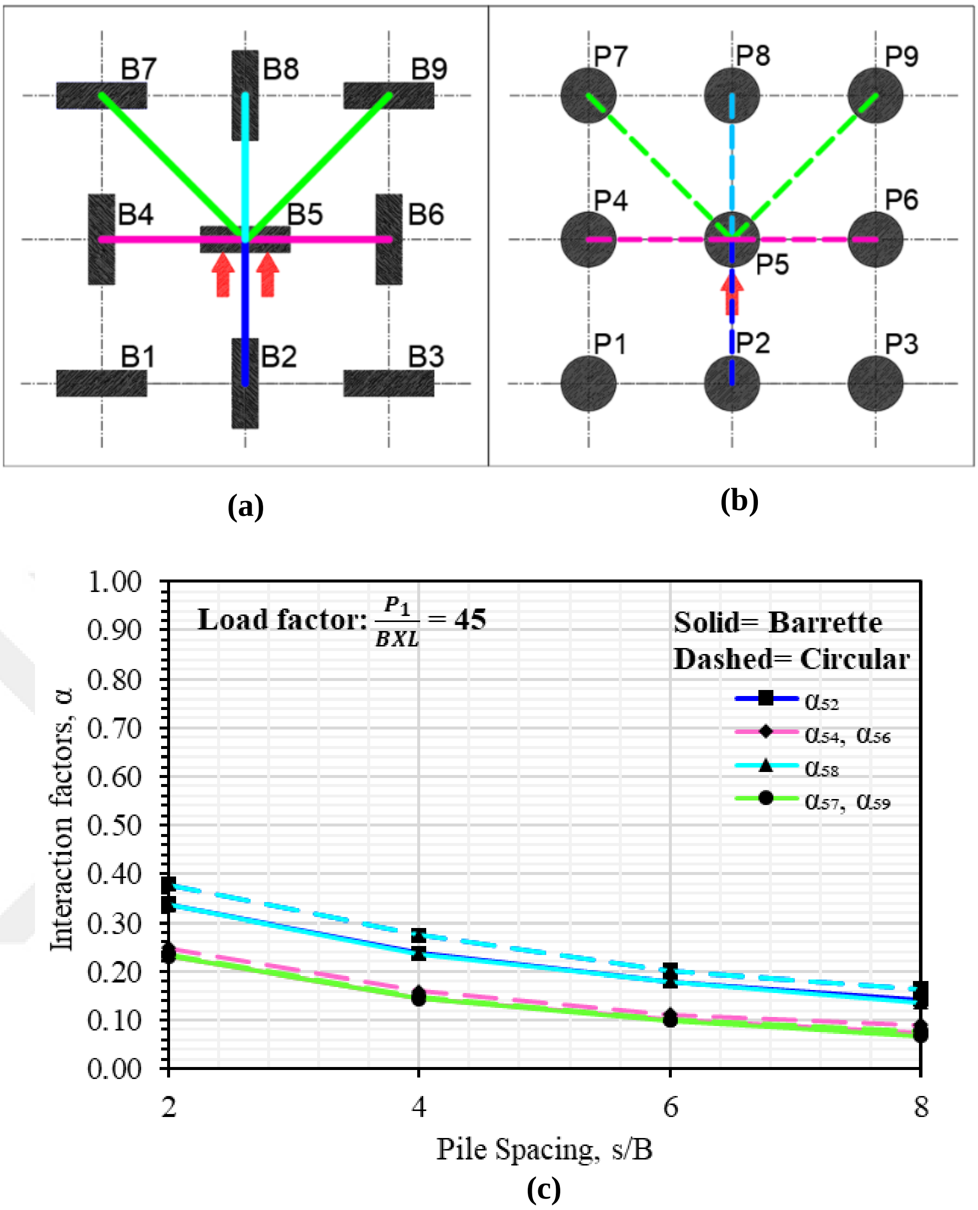

Figure 4.4 (a) y-direction loading of barrette pile group, (b) y-direction loading of circular pile group, (c) Comparison of interaction factors for circular and barrette piles in y-direction loading

The receiver pile exhibited larger displacement causing lower computed factors according to Eq. 2.1. In Case-2, however, the source pile has larger stiffness in the loading direction experiencing smaller displacement leading to higher interaction factors. Another aspect of barrette and circular pile group comparison is that the flexibility matrix is no longer symmetric for barrette piles whereas it is the opposite for circular piles. It may be concluded that what matters in elastic three-dimensional pile group analyses is the relative stiffness between the source and receiver piles.

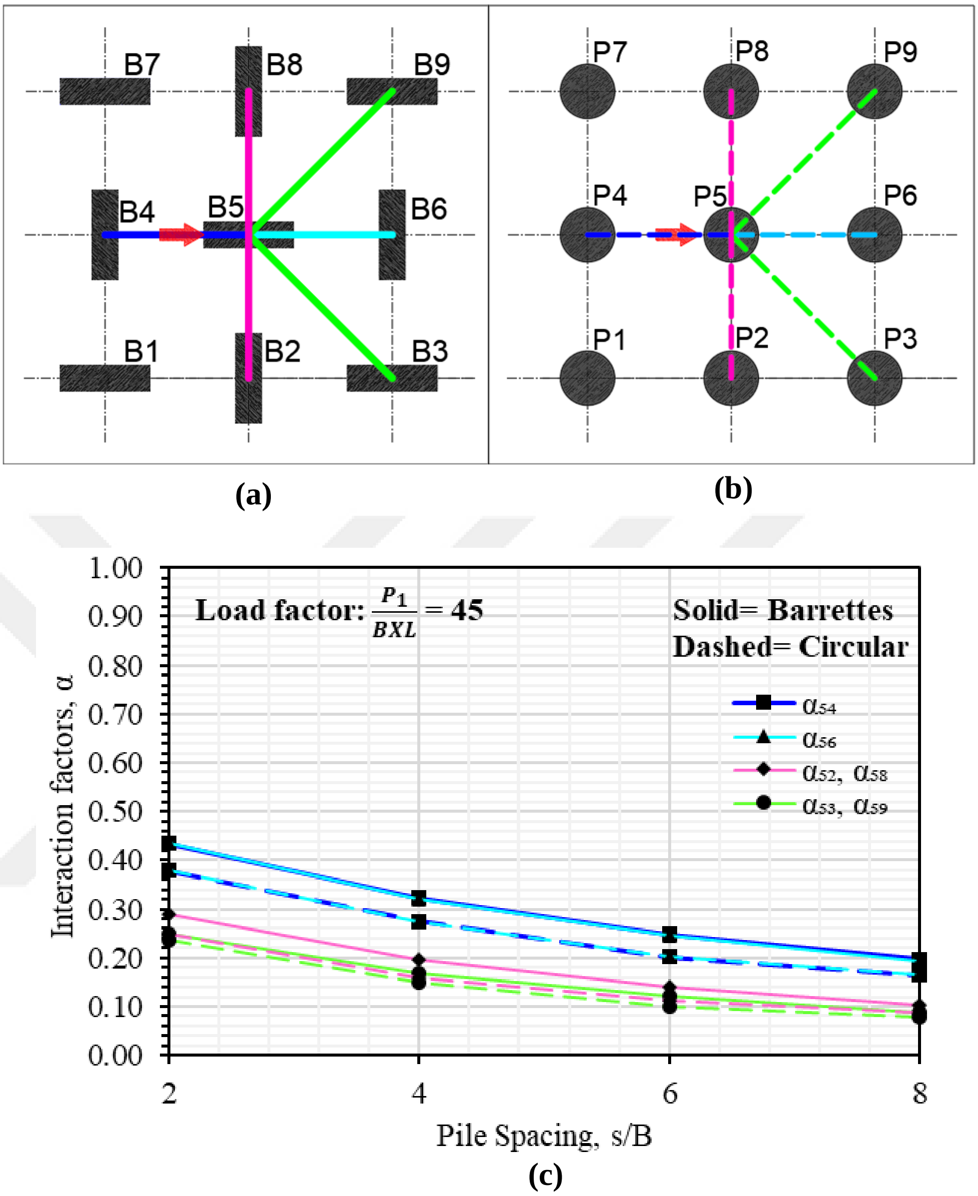

Figure 4.5 (a) x-direction loading of barrette pile group, (b) x-direction loading of circular pile group, (c) Comparison of interaction factors for circular and barrette piles in x-direction loading

4.2 3D Numerical Analyses with Nonlinear Soil Model

4.2.1 Free Head Group Piles

Interaction factors were determined depending on pile orientation for rectangular cross-sections since loading the piles varied depending on the position of each receiver pile, as shown in Figure 4.6. As one may follow on the figure that there were two cases named as Case-1 and Case-2 each having four sub-cases depending on the position of the source piles as shown in Figure 4.7a and Figure 4.8a

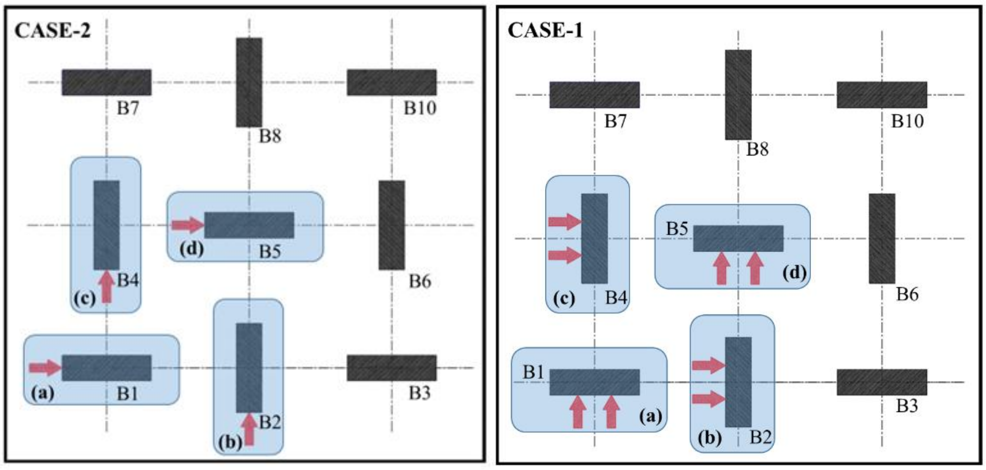

Figure 4.6 Case-1 (loading along minor pile axis); Case-2 (loading along major pile axis)

A double layer soil profile was considered and influence of soil density on barrette pile response was studied by changing the ratio of the stiffness of upper layer to that of the lower one (E_{upper}/E_{lower}). This ratio was adjusted as 0.25, 0.50, 0.75 and 1.0 for soil relative densities in upper layer being RD=25%, RD=50%, RD=%80 and RD=100%, respectively. Therefore, the relative density of lower soil layer was kept constant as RD=100% during the analyses. The thickness of the upper layer (h_1) was arranged such that it was equal to 0.125h (5m), h (40m) being the total thickness of the soil profile as illustrated on Figure 3.1.

The source pile was loaded by means of a distributed surface lateral load at the pile head increasing up to 300 kPa with 100 kPa increments for an 80x280 barrette pile (P1=100, P2=200, and P3=300 kPa). The dimensionless load factor was defined as E_{upper}/P.

Analyses revealed that the location and orientation of the receiver pile with respect to the source played an essential role on the lateral interaction factors. This may be better explained by the help of Case-1d and Case-2d, where source piles are located at the center of the 3x3 pile group as shown in Fig. 4 and Fig. 5 where the soil profile consists of a single sand layer with a relative density of 100%. It was found that whether the major axis of the receiver pile was parallel or perpendicular to the loading direction made the largest difference in pile response. While investigating the influence of pile position, it was noticed that the piles diagonal, adjacent, or behind the source exhibited much lower interaction factors (Figure 4.7b and Figure 4.8b). Sub-cases a, b and c also yielded similar results.

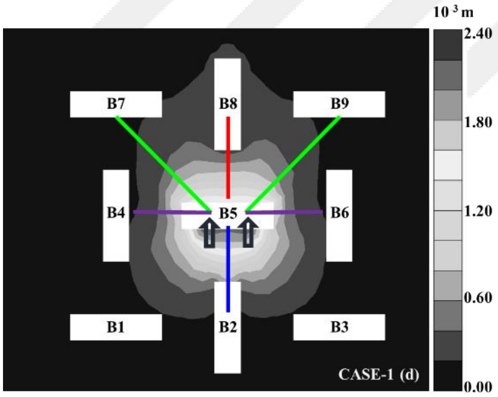

(a)

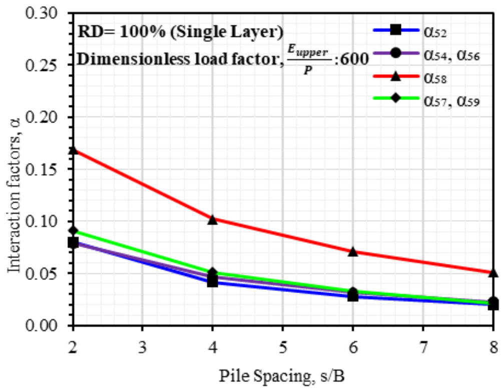

(b)

Figure 4.7 (a) Soil displacement distribution in Case-1d, (b) Interaction factors between source pile B5 and receiver piles in Case-1d.

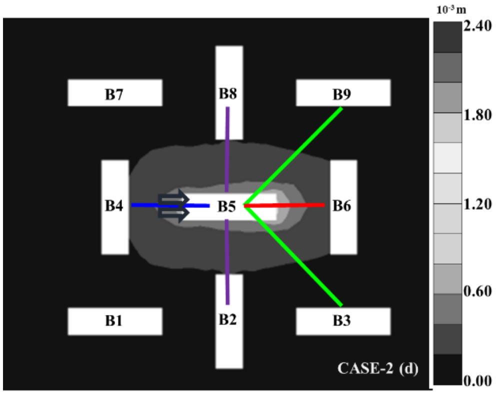

(a)

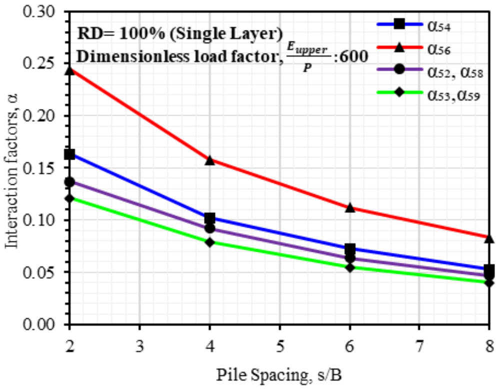

(b)

Figure 4.8 (a) Soil displacement distribution in Case-2d, (b) Interaction factors between source pile B5 and receiver piles in Case-2d.

The given figures show that what dominates the interaction factor is the orientation of the piles with respect to each other and the way the interaction factor is defined as given in Eq. 2.1. The fact that interaction factors computed for neighboring piles in Case-2d are larger than those for Case-1d can be attributed to the higher inertia of the source pile in Case-2d. The source pile loaded along its stronger axis exhibited smaller displacements in this case. It is interesting to note that the receiver pile yielded larger displacements than that of Case-1d just because its stronger axis was oriented orthogonal to the source.

Similar behavior exists for soils with different relative densities. One may notice in Figure 4.9 that interaction between the source and the leading pile considerably decreases with soil density. Taking a closer look at Figure 4.10 in which comparisons among double layer soil cases are given, the presence of looser soil in the upper layer (h_1=5 m, Figure 3.1) results in a decrease on the interaction factors. This behavior shall be attributed to the nonlinear soil response which is reflected even in smallest head loading same behavior was also mentioned by Kimberly et. al (Kimberly et al. 2022). The largest interaction factors are computed for the RD=100% case (i.e., the piles are completely embedded in a single layer) as expected.

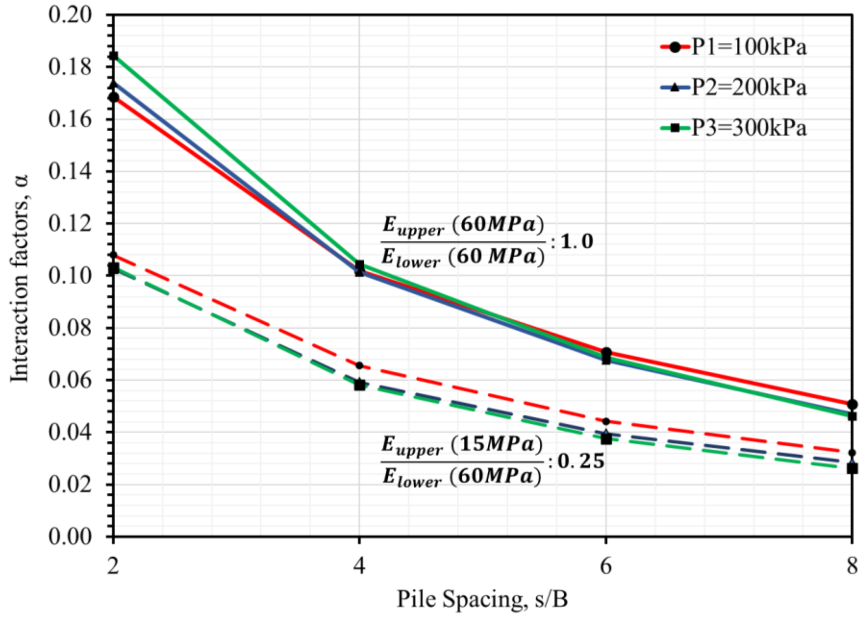

Figure 4.9 Effect of loading intensity on interaction factors between the source and the leading pile (Interaction factors between piles B5 and B8 in Case-2 (d))

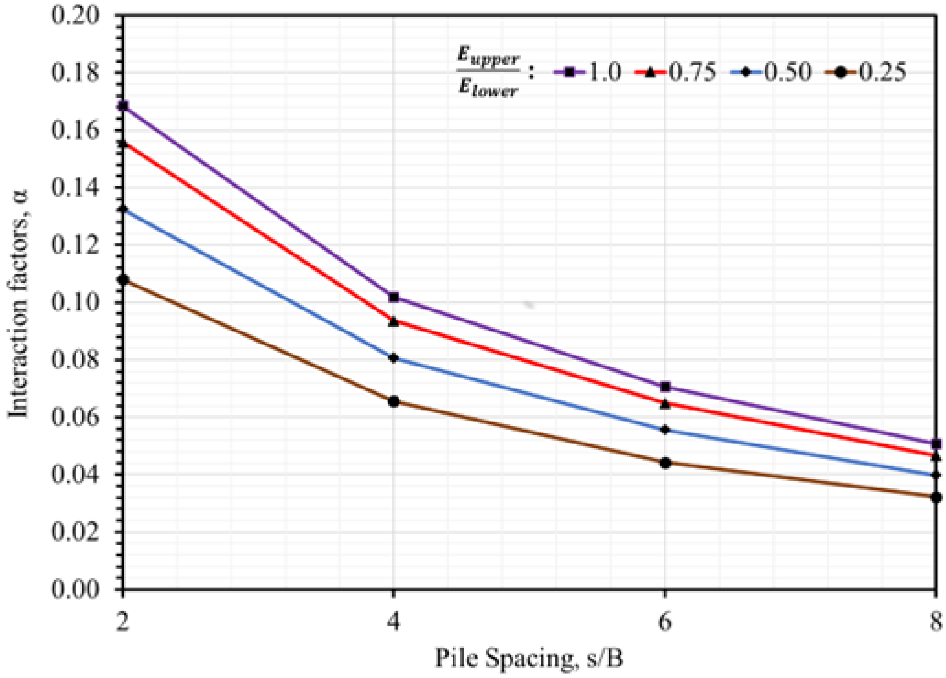

Figure 4.10 Effect of soil density on interaction factors between the source and the leading pile (Interaction factors between piles B5 and B8 in Case-2 (d))

An important aspect of pile geometry on achieved results is that the flexibility matrix to be formed using the interaction factors would not be symmetric whether this soil is assumed to behave elastic or nonlinear. Analyses results indicate that the group effect for barrette piles is considerably different than it is for circular piles.

The interaction factors computed for the 3x3 circular and barrette pile groups are compared in Figure 4.11 and Figure 4.12. It should be mentioned that the edge-to-edge spacing between two piles in a group is the same for both cases. It has been stated above that the interaction between the barrette piles varies according to the position and orientation of the pile positioned in front of the loaded pile. The interaction factors obtained for the barrette pile group in Case-1d and Case-2d are compared with those of circular piles. Interaction factors computed for circular piles with an equivalent area are not affected by the disposition of the piles as they have the same inertia in all directions. The applied loads on the circular pile group given in Figure 4.11b and Figure 4.12b were symmetrical yielding same interaction factors for both cases. Results of these analyses support the idea that inertia of the receiving pile govern the pile-soil-pile interaction mechanism.

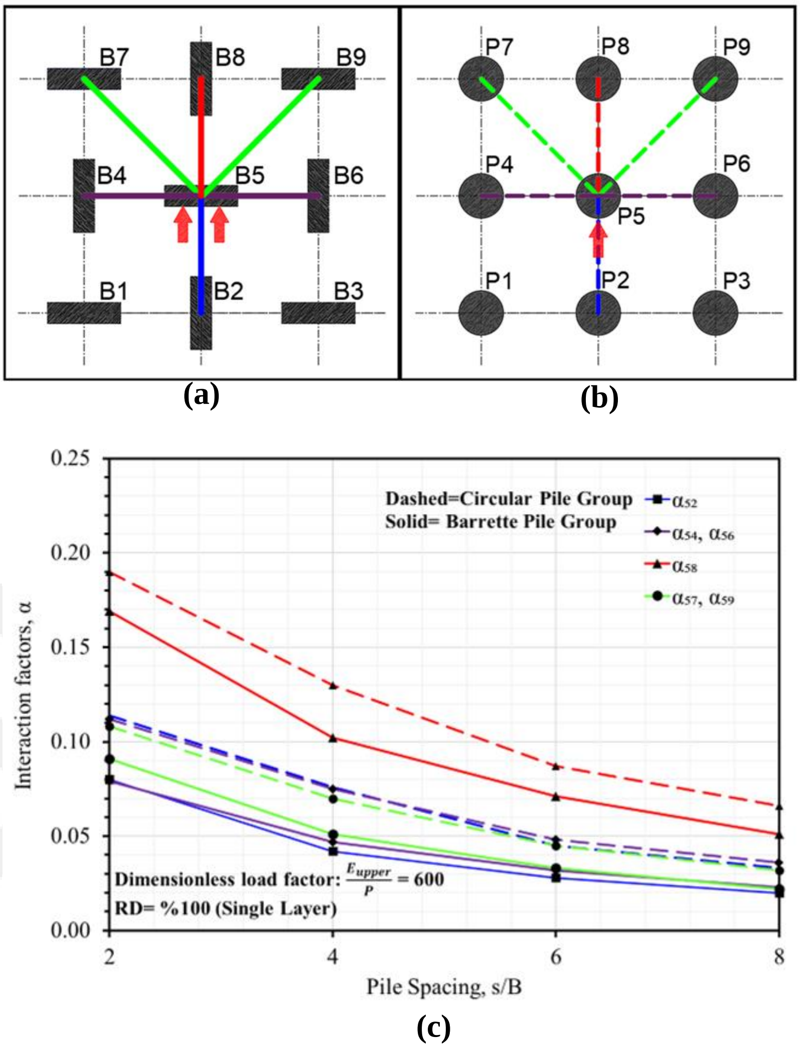

Figure 4.11 (a) Loading in the minor axis direction of pile B5; (b) Loading in the minor axis direction of pile P5; (c) Comparison of interaction factors for circular and barrette piles for loadings along the minor axes

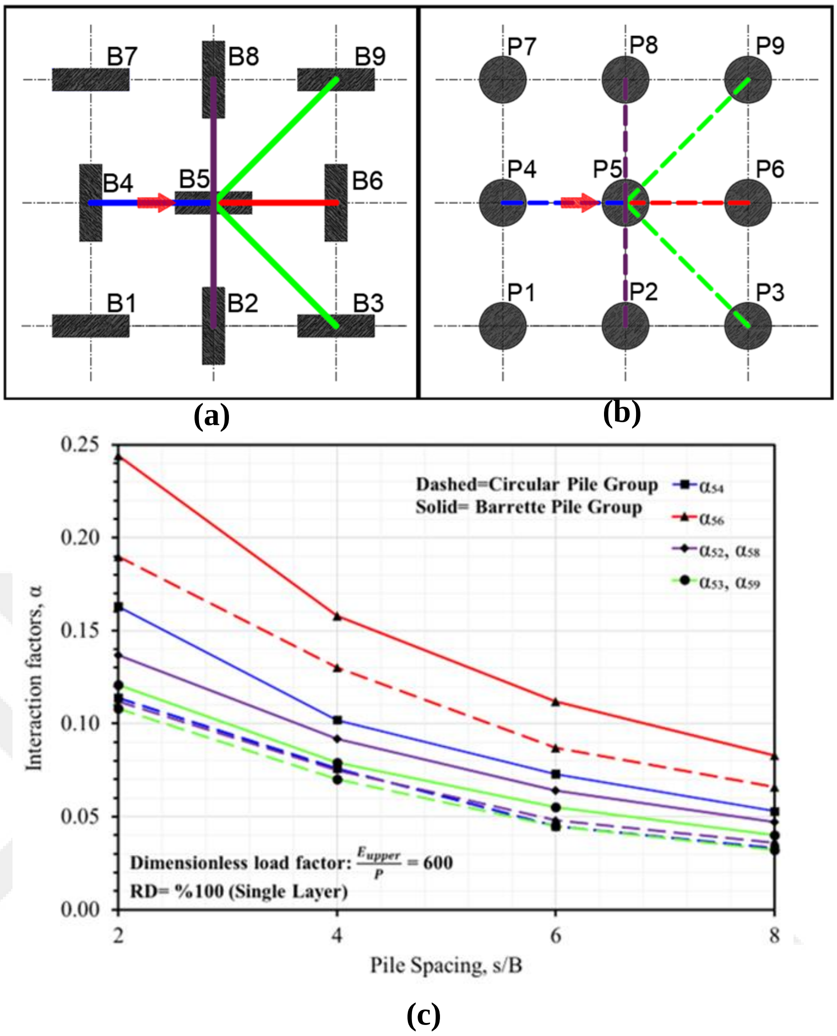

Figure 4.12 (a) Loading in the major axis direction of pile B5; (b) Loading in the major axis direction of pile P5; (c) Comparison of interaction factors for circular and barrette piles for loading along the major axes

4.2.2 Fixed Head Group Piles

It is well known that pile-soil-pile interaction in fixed-head pile groups alter single pile response, and this mechanism is generally known as shadowing effect. By Poulos proposed a methodology that yields lateral load per pile row based on the assumption that piles exhibit same head displacement (Poulos & Davis, 1980). The P-multiplier approach, on the other hand, is the most extensively utilized method to obtain displacement, soil resistance and sectional force distribution along pile length (Brown et al., 1989). Currently, most design offices apply this methodology to groups consisting of circular or square piles. While working with square piles, a slight correction is applied to p-y curves originally developed for circular ones. Although there are studies regarding laterally loaded barrette piles (Zhang, 2003; Choi et al, 2015;), research on p-y curves for barrette piles is scarce (Amar Bouzid, 2018; Poulos et al., 2019) general practice for rectangular piles is still to assume an equivalent diameter and then follow the same methodology to consider shadowing effect.

In order to analyze the shadowing effect on the barrette pile group, a 4x4 fixed-head barrette pile group was created with a rigid plate serving as the pile cap in the model. The pile group was then laterally loaded by defining a surface traction ranging between 20 and 100 kPa with 20 kPa increments. The aspect ratio of the pile cross-section was set as L/B=3.5, where L and B stand for length and width of the pile section, respectively. In order to provide complete pile head fixity between the cap and the piles 10 pieces of rigid embedded beam portions were placed for each pile. The optimum number of such embedded beam elements were decided upon several trials until rotation of the pile heads were avoided. The success of this modelling stage was also checked by comparing the sum of the lateral loads shared by each pile with the total applied load at the cap. A two-layer soil profile was considered for which the relative density of the upper layer was set to one half of the below layer (RD=100%). The assigned parameters to each layer are given in the Table 3.2. The thickness of the upper layer (h_1) was kept constant being equal to 0.25h (i.e., 10 m) where h was 40m total thickness of the soil profile as shown in Figure 3.3 and Figure 3.4. The deflected shape of the 4x4 fixed-head pile group is shown in Figure 3.4 proving that full pile head fixity was achieved.

Analyses that were conducted on fixed head pile group revealed that soil arching played an important role on load share among pile rows in addition to the pile orientation. It can be seen that soil arching is especially acting between first and second pile rows. This mechanism is shown in Figure 4.13 on which lateral stress distribution along x-axis (σ'_{xx}) is given along with lateral displacement distribution. It may be noticed on this figure that the leading pile row is capable of generating arching with a major contribution from B4 and B12 piles. Stress increase towards both sides of the piles is observed with a minor variation at the B4 pile located at the lower right hand-side corner of the group. This may be attributed to the lack of a neighboring pile as opposed to the inner located B12 pile. It is believed that presence of piles with varying bending stiffness has an influence on load distribution in a group (Figure 4.14) as well. Average loads shared by each pile type are presented in Figure 4.14 where piles are numbered with respect to their head loads. The leading row piles distinguish themselves from the rest of the group as they attracted larger loads. What is remarkable on the average sense is that piles attained loads with respect to their acting bending stiffness along the direction of lateral loading and their position in the group. Therefore, the piles are tagged in four groups. The piles tagged as ‘Pattern-1’ in the leading row received highest load with their major axis parallel to the loading direction. As one may notice in Figure 4.14 that there is a slight decrease in load sharing ratio (H/H_{avg}) with pile spacing. Load sharing is defined as the ratio of the load computed at the pile head (H) to the average load that would act at the head of each pile if the total load, H_{total}, is distributed equally among the pile (i.e. $H_{avg}=H_{total}/N_{piles}$). In terms of load sharing ratio Pattern-2 comes next with piles’ major axis being parallel to the loading. This group of piles, however, does not pose a significant reduction with pile spacing. Pile groups consisting of lowest bending stiffness with respect to the loading (i.e., minor axis parallel) shared smallest loads as expected. It appears that load distribution because of arching and shadowing effect played a considerable role for the leading row. Bending stiffness that is active along the loading direction is more effective in terms of load sharing for the trailing rows. The position of the piles in the 4x4 group has also played a role reflecting influence of shadowing mechanism.

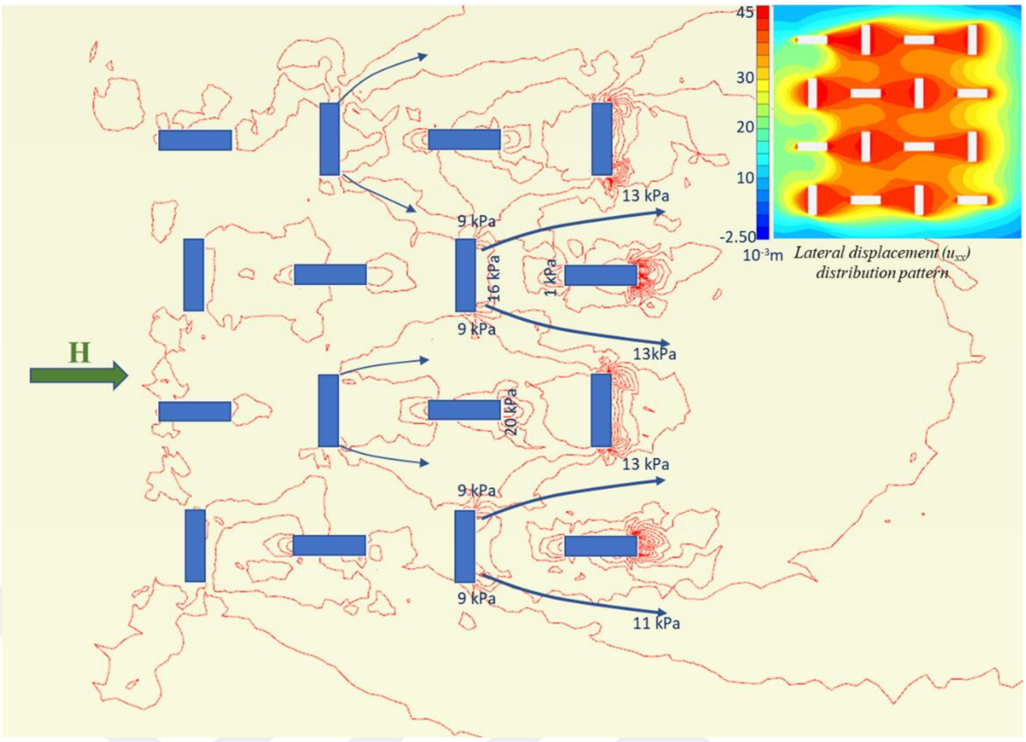

Figure 4.13 Horizontal stress (σ′xx) and lateral displacement distribution pattern

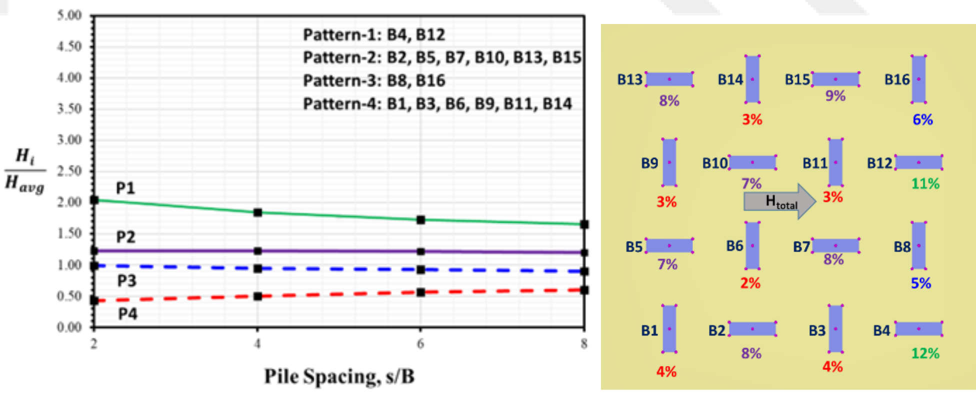

Figure 4.14 Pile head load distribution for a fixed head 4x4 barrette pile group

Lateral load-displacement curves (p-y curves) were deduced for edge-to-edge pile spacing of s=4B by acquiring effective normal and shear stresses acting on the interface elements assigned to each pile as shown in Figure 4.15. Shear stresses on side surfaces and the normal stress on the front face of the pile contributes the passive soil resistance, whereas the stress on the back face constitutes the active soil thrust. The net passive soil resistance ($p_{net} = \sigma_1 + 2\tau_1 - \sigma_2$) per unit length of the pile was used while establishing p-y curves. Two different depths being 1m and 5m below the surface were chosen while driving the curves in a double layered soil layer where the upper layer consists of medium dense sand (RD=50%) leading to a stiffness ratio of E_{upper}/E_{lower}=0.5. The pile was half length embedded (h/L_{pile}=0.5) to the lower very dense soil. Two groups of piles were taken into consideration during the analyses. The first group involved piles from each row with major axis parallel to the loading, whereas the minor axis of the piles was parallel to the loading in the second group as shown in Figure 4.16. Accordingly developed p-y curves are given in Figure 4.17 and Figure 4.18 where they are compared with API based curves. On the same figure p-y curves belonging to single barrette pile are also provided. The p-multipliers for the leading and trailing rows are presented in Table 4.1. One may notice in Table 4.1 that the multipliers are not the same with those given in the literature (Brown et al, 1987; McVay et al, 1998; Ruesta&Townsend, 1997) indicating that shadowing mechanism is quite different than circular pile groups. The API curves according to equivalent circular pile yielded much larger soil resistances since the API procedure is based on smaller diameter steel pipe piles (Achmus, 2017).

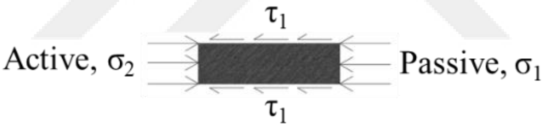

Figure 4.15 Stress distribution scheme on an interface element

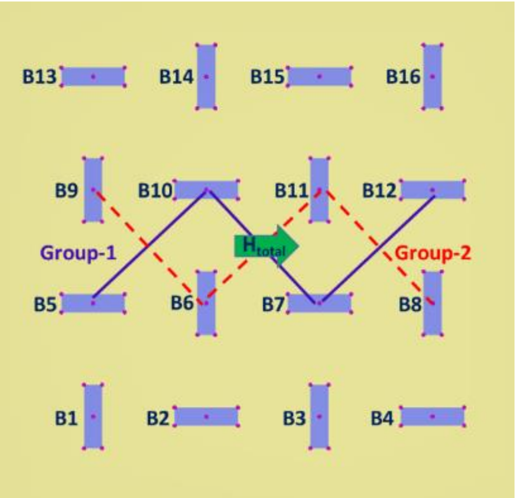

Figure 4.16 Pattern 1 and 2 based on barrette pile position

Table 4.1 Computed p-multipliers (p/p_{single}) and their comparison with the literature

Pile group	d (m)	1st row	2nd row	3rd row	4th row	Rollins et al. (2005)			
						1st	2nd	3rd	4th
No.1	1.0	0.93	0.24	0.14	0.10	0.92	0.88	0.82	0.79
	5.0	0.82	0.34	0.19	0.19				
No.2	1.0	0.91	0.40	0.25	0.20				
	5.0	0.53	0.17	0.11	0.11				

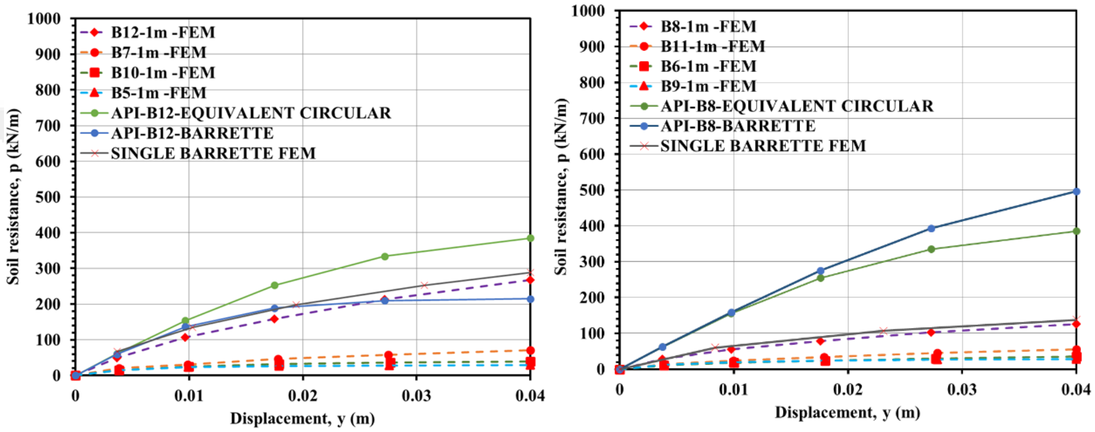

Figure 4.17 p-y curves 1.0m below the surface (a) Group-1 (b) Group-2

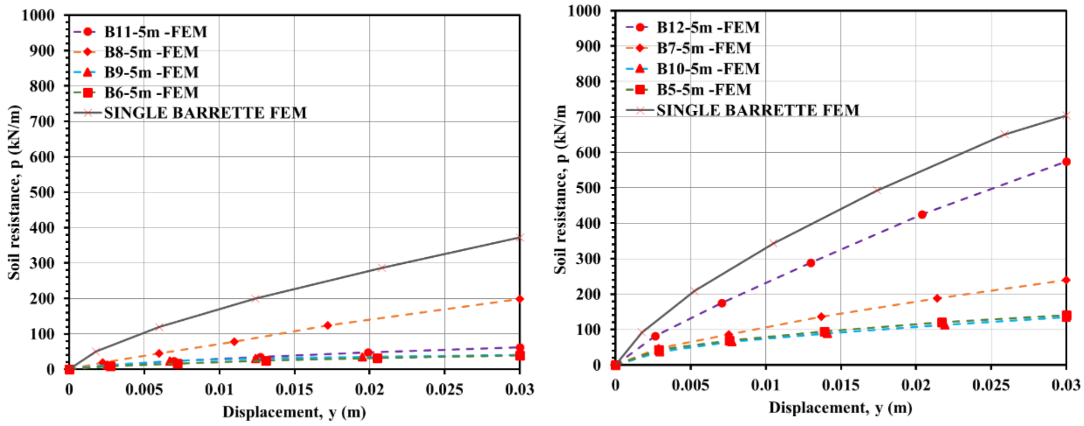

Figure 4.18 p-y curves 5.0m below the surface (a) Group-1 (b) Group-2

CHAPTER FIVE
CONCLUSIONS

5.1 Conclusions and Recommendations

In this thesis, the pile-soil-pile interaction aspects for horizontally loaded barrette pile groups were studied based on numerical analysis models. While establishing the models, orientation and spacing of the piles in a group were set as basic variables. Soil layers in a double layer profile were assumed as cohesionless at different relative densities, and analyses were conducted assuming linear and nonlinear soil response. Besides, the piles were either fixed or left as free head in a group. Achieved results and recommendations for further studies are presented in the following:

i. Since barrette piles have rectangular cross-sections, the most critical factor in their interaction is the pile's potential in resisting the induced displacement along the loading direction. This potential is found to be strongly related with pile's bending stiffness. Considering that the interaction factor between any two piles is defined as the ratio of the displacement of the leading pile (i.e. the receiver pile as denoted inside the text) to that of the source pile (i.e. the head loaded pile) the pile that resists the loading with its stronger axis greatly affects the value of the interaction factor. This influence is prominent for cases where the receiver pile resists the loading with its stronger axis. Therefore, it can be said that piles' orientation in a group is one of the critical factors for pile-soil-pile interaction.

ii. Comparing the response of the circular and barette piles, it can be said that groups with rectangular pile sections behave quite different than circular piles. First of all, the stiffness matrix becomes unsymmetric due to pile orientation. This statement holds for both elastic and nonlinear soil conditions. Circular piles in a group, on the other hand, yield always symmetric stiffness matrix for elastic soil conditions. Shadowing effect is much more pronounced for barette piles.

iii. It is interesting to note that influence of soil’s relative density on pile response is also related to the pile’s embedment depth inside the underlying dense sand. In other words, the thickness of the upper layer is quite critical on pile deformation pattern. For loose soil conditions, the sand in front of the pile is easily brought into passive soil conditions and applied load is transferred to deeper dense sand. If the thickness of the upper layer increases, the displaced passive wedge in the front widens yielding larger interaction factors between the leading and source piles since a larger amount of soil mass acts on the receiver pile. In this case, the pile tends to bend around a deflection point and consumes a larger amount of the applied load along its depth as the loose soil gets thicker. This effect is reduced as soil density increases and disappears when the relative density of upper and lower layers become equal (i.e., RD=100%). The source pile becomes more capable of transferring the applied load to the receiver pile for homogeneous and denser soil conditions.

iv. It is considered that the relative stiffness of the pile with respect to the surrounding soil governs the soil-pile interaction and shadowing effect between the piles. This may be expressed by the active length concept which is not the same along weaker and stronger axes of the barette.

v. The active length of piles with smaller inertia in the loading direction is shorter, and the load transferred to the surrounding soil is limited below the critical depth. On the other hand, piles with larger inertia in the loading direction have longer active lengths and transfer loads to deeper depths. As the critical depth increases, the head load required for the same lateral displacement increases resulting in larger soil resistance.

vi. According to the analyses results, the barrette piles' geometry is significant in determining the lateral load-displacement relationships (i.e. p-y curves). It is incorrect to adopt p-y curves that were in use for circular piles to barrette piles. It is found that developing p-y curves for an equivalent diameter circular section in lieu of a rectangular pile does not have much basis. The p-y multipliers for barette piles are also different than those of the circular ones. In the design of barrette piles under lateral loads, more detailed analyses should be made, and, if necessary, p-y curves should be obtained for each barrette pile separately.

vii. Three-dimensional numerical analyses for pile foundations with rectangular sections are needed since soil nonlinearity and pile orientation effects cannot be handled safely by assuming an equivalent circular section.

viii. Numerical analyses may be extended to cover larger pile groups and soil combinations. Dynamic pile-soil-pile interaction may be studied for barette piles. It is expected that dynamic interactions factors would be different like the static loading case.

ix. Experimental model studies would be beneficial in understanding soil-pile interaction and shadowing effect for barette pile groups.

x. Sectional dimensions of the barrette piles were fixed at L/B=3.5 in the research. L/B ratios other than 3.5 may also be studied in future research to gain more insight on the influence of pile flexibility on pile-soil-pile interaction.

REFERENCES

Ashour, M.; Norris, G., &Pilling, P. (2001). Assessment of pile group response under lateral load. *International Conferences on Recent Advances in Geotechnical Earthquake Engineering and Soil Dynamics, 5. March, San Diego-California*

Amar Bouzid, D. (2018). Numerical investigation of large-diameter monopiles in sands: Critical review and evaluation of both API and newly proposed p-y curves. *International Journal of Geomechanics, 18*(11), 04018141.

Banerjee, P. K., & Davies, T. G. (1978). The behaviour of axially and laterally loaded single piles embedded in non-homogeneous soils. *Geotechnique*, *30*(1), 88–92.

Basu, D., Prezzi, M., Choi, Y. S., & Salgado., R. (2015). Study on laterally loaded piles with rectangular and circular cross sections. *Geomechanics and Geoengineering*, *10*(2), 139-152.

Benz, T. (2006). *Small-Strain Stiffness of Soils and its Numerical Consequences* (PhD., Thesis), Universität Stuttgart.

Bradley, B. A., Cubrinovski, M., & Dhakal, R. P. (2008). Performance-based seismic response of pile foundations. *ASCE 4th Geotechnical Earthquake Engineering and Soil Dynamics Conference, Sacramento, California*, 1–11.

Brinkgreve, R. B. J., & Engin, E. (2010). Validation of empirical formulas to derive model parameters for sands. *7th NUMGE Conference, June, Trondheim Norway.*

Brown, B. D. A., Morrison, C., & Reese, L. C. (1989). Lateral load behaviour of pile group in sand. *International Journal of Rock Mechanics and Mining Sciences & Geomechanics Abstracts, 26*(3–4), A145.

Brown, D.A., Morrison, C., & Reese, L.C. (1988). Lateral load behaviour of pile group in sand. *Journal of Geotechnical Engineering, ASCE, 114*(11), 1261–1276.

Brown, D.A., Reese, L.C., & O'Neill, M.W. (1987). Cyclic lateral loading of a large-scale pile group. *Journal of Geotechnical Engineering, ASCE, 113*(11), 1326–1343.

Duncan, J.M. & Chang, C. Y. (1970). Nonlinear analysis of stress and strain in soils. *Journal of the Soil Mechanics and Foundations Division, 96*(5), 1629-1653

Kaynia, A., & Kausel, E. (1980, February 10). *Dynamic stiffness and seismic response of sleeved piles.* TRID Database. https://trid.trb.org/view/162450

Kramer, S. L., Valdez, C., Blanchette, B., & Baker, J. W. (2014). Performance-based design factors for pile foundations. *WSDOT Research Report, WA-RD 827.1.*

Kimberly J., Min S., Cheng L. (2022). Numerical analysis of group effects of a large pile group under lateral loading. *Computers and Geotechnics, 114,* 104660.

Achmus M., Akdag C.T., Thieken K. (2013). Load-bearing behavior of suction bucket foundations in sand. *Applied Ocean Research, 43,* 157-165

McVay, M., L. Zhang, T. Molnit & P. Lai. (1998). Centrifuge testing of large laterally loaded pile groups in sands. *Journal of Geotechnical and Geoenvironmental Engineering, ASCE 124*(10), 1016–1026.

Mylonakis, G., & Gazetas, G. (1998). Settlement and additional internal forces of grouped piles in layered soil. *Geotechnique, 48*(1), 55–72.

Plaxis B.V. (2019, September 1). *Geotechnical Engineering Software Company. Delft, Netherlands.* https://www.bentley.com/en/products/brands/plaxis

PLAXIS3D. (2019, September 5) *Geotechnical Engineering Software.* Plaxis B.V., Delft, Netherlands. https://virtuosity.bentley.com/product/plaxis-3d

Poulos, H. G. (1968). Analysis of the settlement of pile groups. *Geotechnique, 18*(4), 449–471.

Poulos, H. G. & Davis, E. H. (1980). *Pile Foundation Analysis and Design Book* (Chapter 7-8). Wiley .

Poulos, H. G. (1979). Group factors for pile-deflection estimation. *ASCE, Journal of the Geotechnical Engineering Division, 105*(12), 1489–1509.

Poulos, H. G., Chow, H., & Small, J. (2019). The use of equivalent circular piles to model the behaviour of rectangular barrette foundations. *Geotechnical Engineering Journal of the SEAGS & AGSSEA, 50*(3).

Randolph, M. F., & Wroth, C. P. (1979). An analysis of the vertical deformation of pile groups. *Geotechnique, 29*(4), 423–439.

Rao, S. S. (2004). *The finite element method in engineering*. Elsevier Science & Technology Books.

R. D, Mindlin. (1951). Influence of rotatory inertia and shear on flexural motions of isotropic, elastic plates. *ASME Journal of Applied Mechanics, 18,* 31–38.

Rotta Loria, A. F. (2018). Performance-based design of energy pile foundations. *DFI Journal - The Journal of the Deep Foundations Institute, 12*(2), 94–107.

Ruesta, P.F., and Townsend, F.C. (1997). Evaluation of laterally loaded pile group at Roosevelt bridge. *Journal of Geotechnical and Geoenvironmental Engineering, ASCE, 123*(12), 1153–1161

Schanz, T., Vermeer, P. A., & Bonnier, P. G. (1999). The hardening soil model: formulation and verification. *Beyond 2000 in computational geotechnics: 10 years of PLAXIS International; proceedings of the International Symposium beyond 2000 in Computational Geotechnics, Amsterdam, Netherlands.*

Zhang, L. M. (2003). Behavior of laterally loaded large-section barrettes. *Journal of Geotechnical and Geoenvironmental Engineering*, *129*(7), 639–648.

APPENDICES

Appendix-1 The analyses result of Case-1d shows the interaction factor between source pile and receiver piles

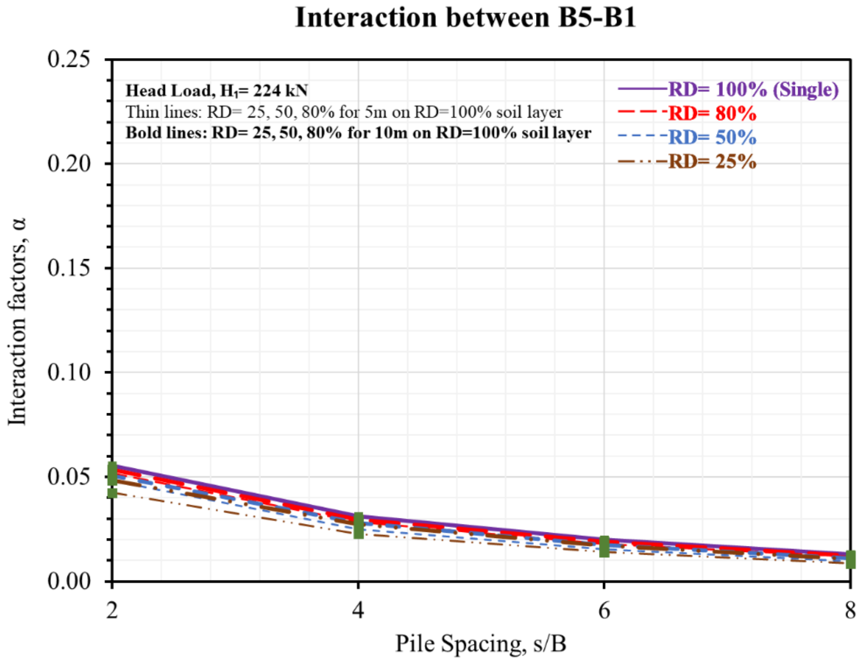

Figure A1.1 The interaction factors in between source pile B5 and receiver pile B1 in Case-1d, Head load on source pile: 224 kN, For two-layer model relative densities of the upper layer, varies 25%, 50%, %80. For single-layer model RD=100%.

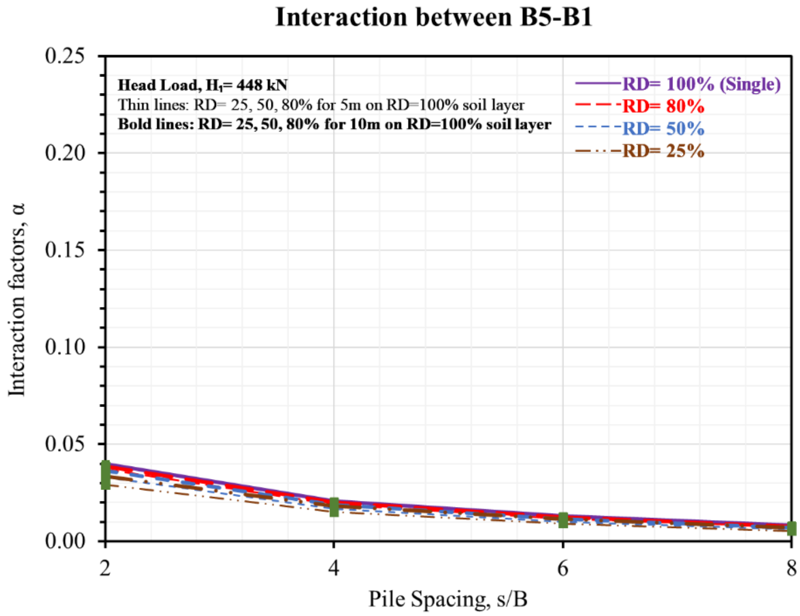

Figure A1.2 The interaction factors in between source pile B5 and receiver pile B1 in Case-1d, Head load on source pile: 448 kN, For two-layer model relative densities of the upper layer, varies 25%, 50%, %80. For single-layer model RD=100%.

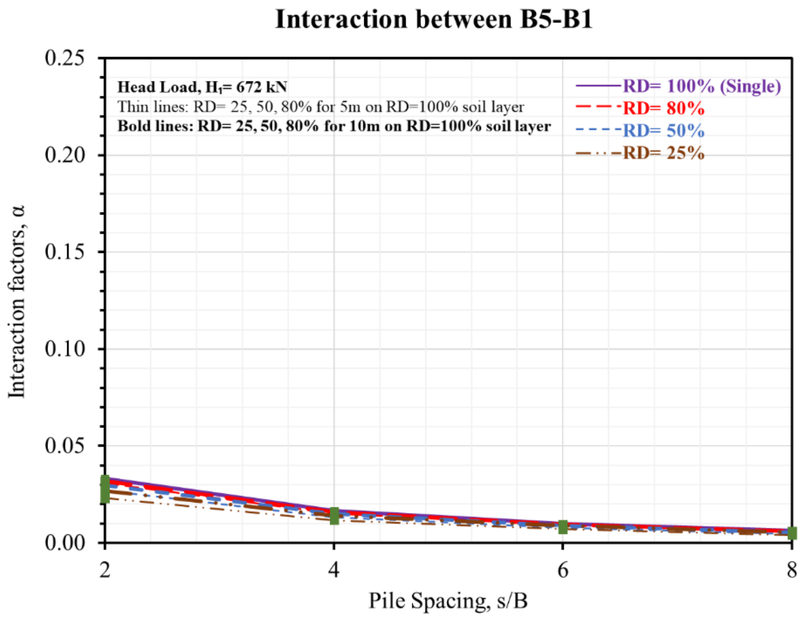

Figure A1.3 The interaction factors in between source pile B5 and receiver pile B1 in Case-1d, Head load on source pile: 672 kN, For two-layer model relative densities of the upper layer, varies 25%, 50%, %80. For single-layer model RD=100%.

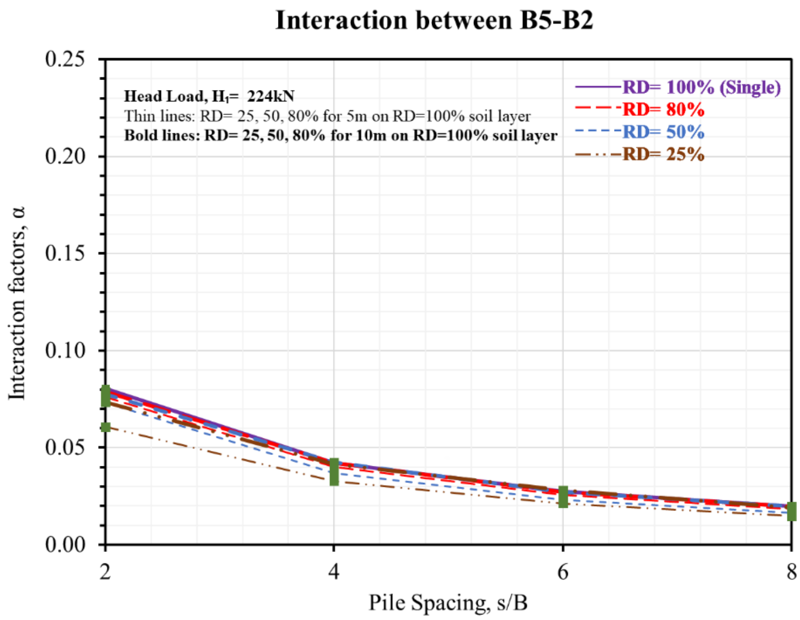

Figure A1.4 The interaction factors in between source pile B5 and receiver pile B2 in Case-1d, Head load on source pile: 224 kN, For two-layer model relative densities of the upper layer, varies 25%, 50%, %80. For single-layer model RD=100%.

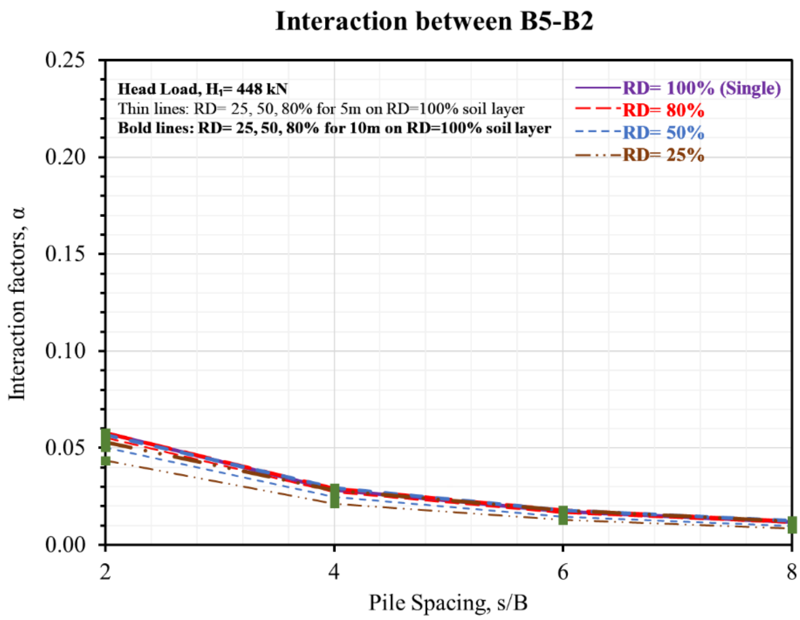

Figure A1.5 The interaction factors in between source pile B5 and receiver pile B2 in Case-1d, Head load on source pile: 448 kN, For two-layer model relative densities of the upper layer, varies 25%, 50%, %80. For single-layer model RD=100%.

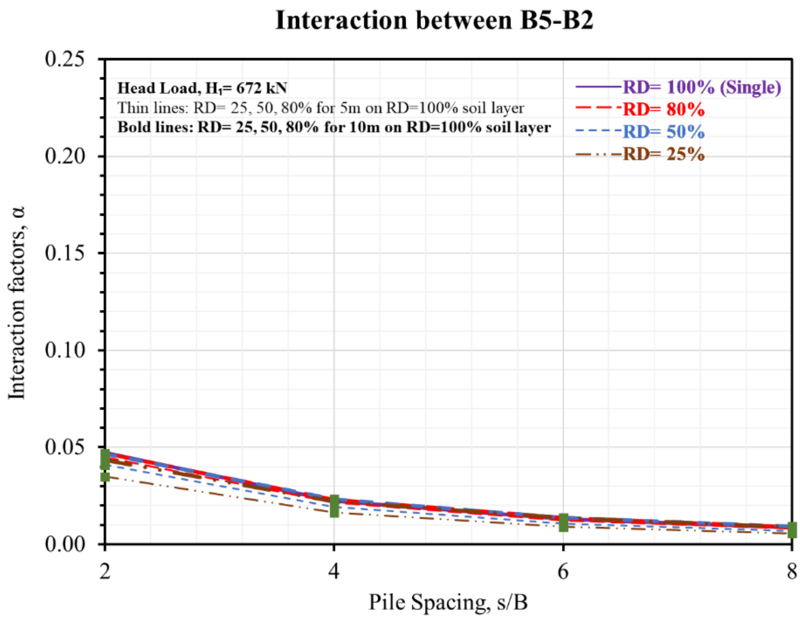

Figure A1.6 The interaction factors in between source pile B5 and receiver pile B2 in Case-1d, Head load on source pile: 672 kN, For two-layer model relative densities of the upper layer, varies 25%, 50%, %80. For single-layer model RD=100%.

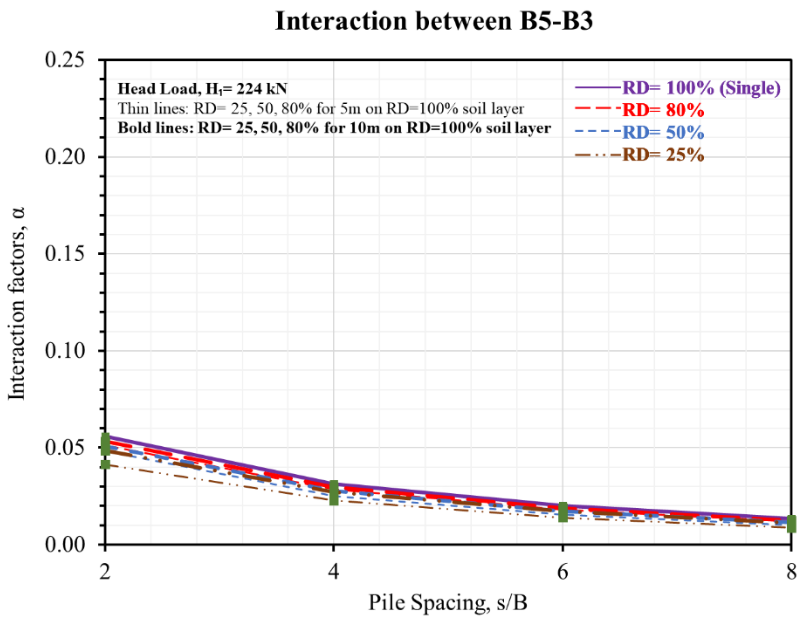

Figure A1.7 The interaction factors in between source pile B5 and receiver pile B3 in Case-1d, Head load on source pile: 224 kN, For two-layer model relative densities of the upper layer, varies 25%, 50%, %80. For single-layer model RD=100%.

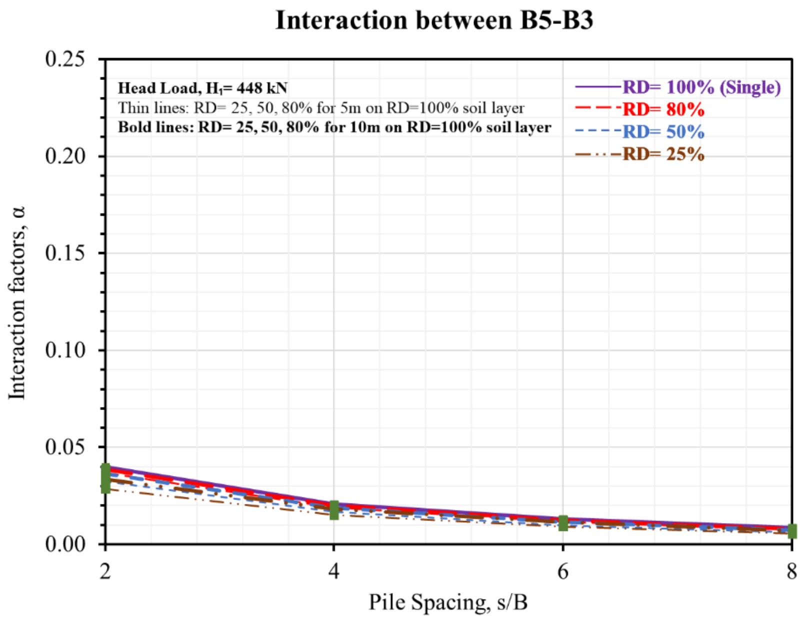

Figure A1.8 The interaction factors in between source pile B5 and receiver pile B3 in Case-1d, Head load on source pile: 448 kN, For two-layer model relative densities of the upper layer, varies 25%, 50%, %80. For single-layer model RD=100%.

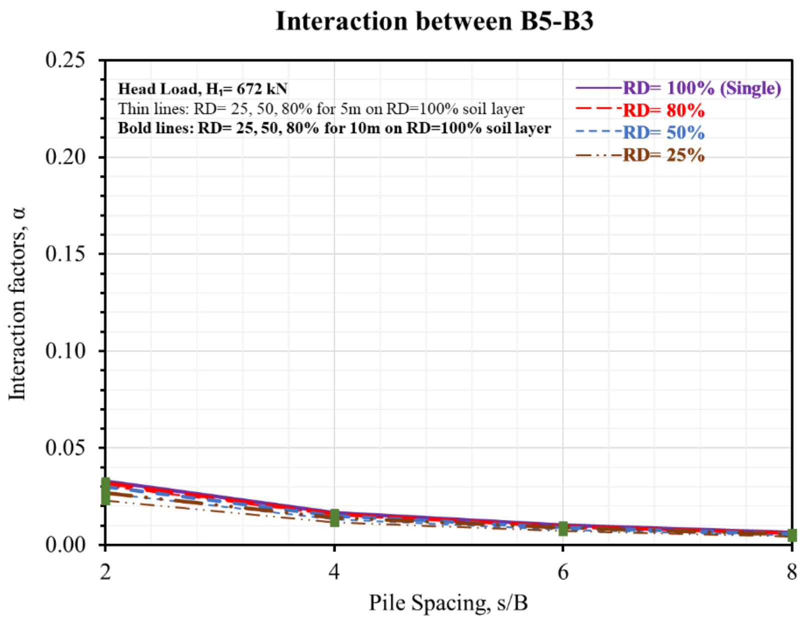

Figure A1.9 The interaction factors in between source pile B5 and receiver pile B3 in Case-1d, Head load on source pile: 672 kN, For two-layer model relative densities of the upper layer, varies 25%, 50%, %80. For single-layer model RD=100%.

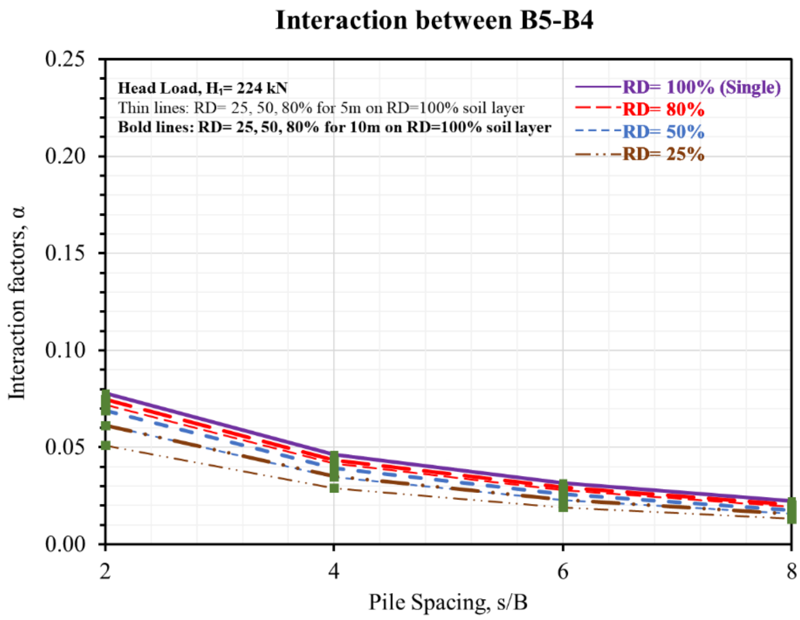

Figure A1.10 The interaction factors in between source pile B5 and receiver pile B4 in Case-1d, Head load on source pile: 224 kN, For two-layer model relative densities of the upper layer, varies 25%, 50%, %80. For single-layer model RD=100%.

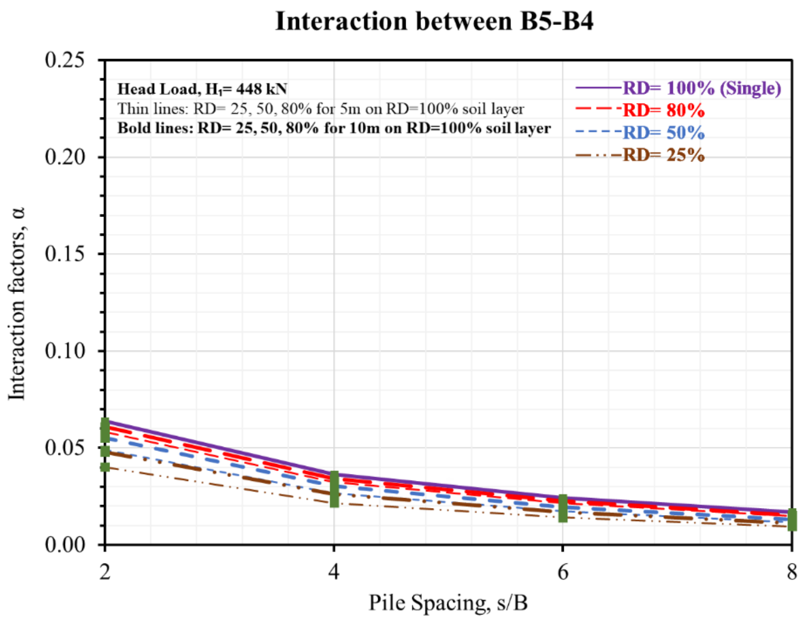

Figure A1.11 The interaction factors in between source pile B5 and receiver pile B4 in Case-1d, Head load on source pile: 448 kN, For two-layer model relative densities of the upper layer, varies 25%, 50%, %80. For single-layer model RD=100%.

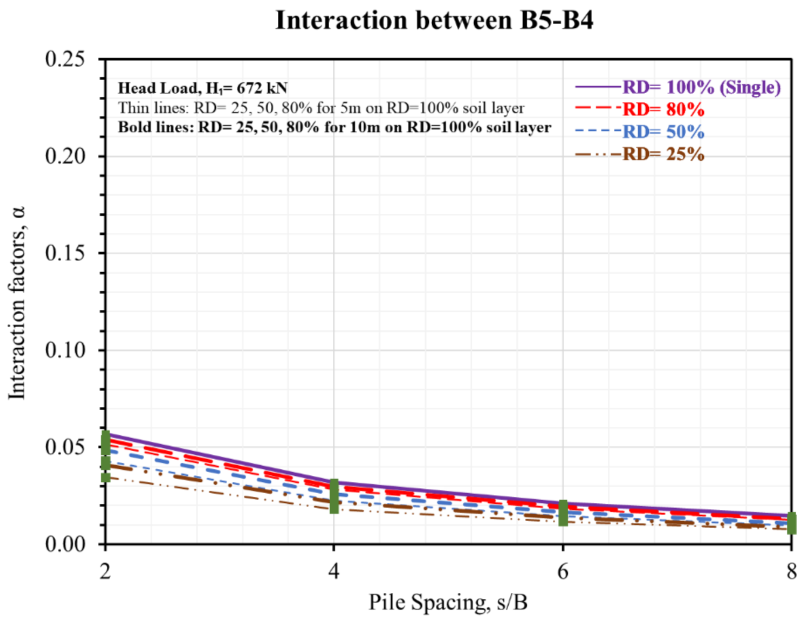

Figure A1.12 The interaction factors in between source pile B5 and receiver pile B4 in Case-1d, Head load on source pile: 672 kN, For two-layer model relative densities of the upper layer, varies 25%, 50%, %80. For single-layer model RD=100%.

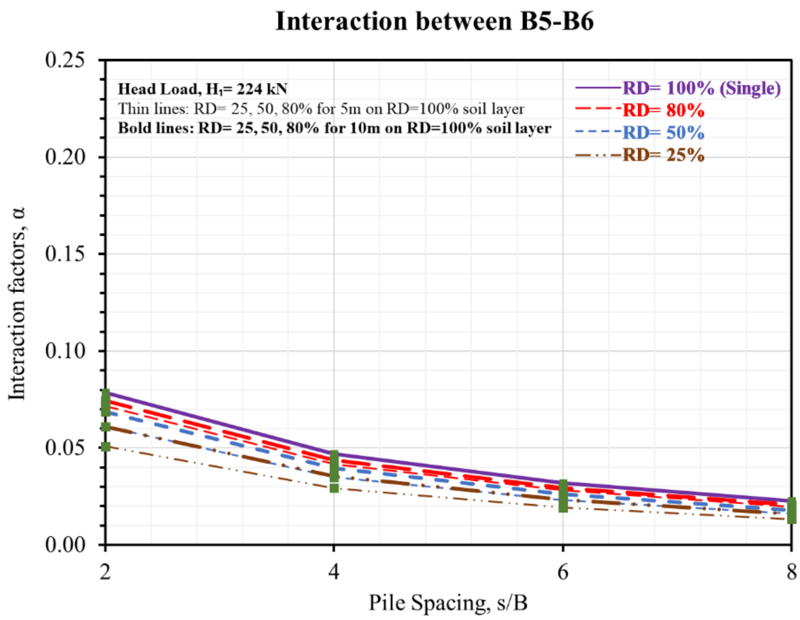

Figure A1.13 The interaction factors in between source pile B5 and receiver pile B6 in Case-1d, Head load on source pile: 224 kN, For two-layer model relative densities of the upper layer, varies 25%, 50%, %80. For single-layer model RD=100%.

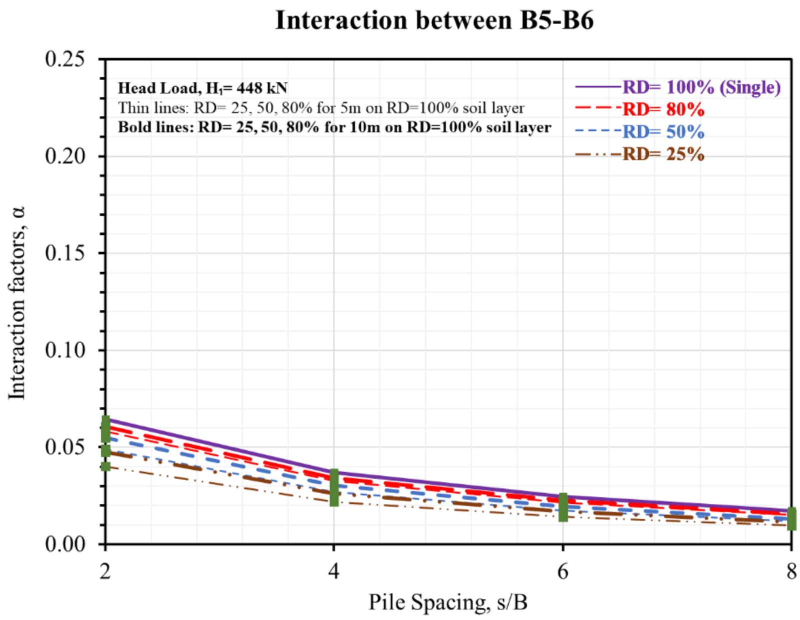

Figure A1.14 The interaction factors in between source pile B5 and receiver pile B6 in Case-1d, Head load on source pile: 448 kN, For two-layer model relative densities of the upper layer, varies 25%, 50%, %80. For single-layer model RD=100%.

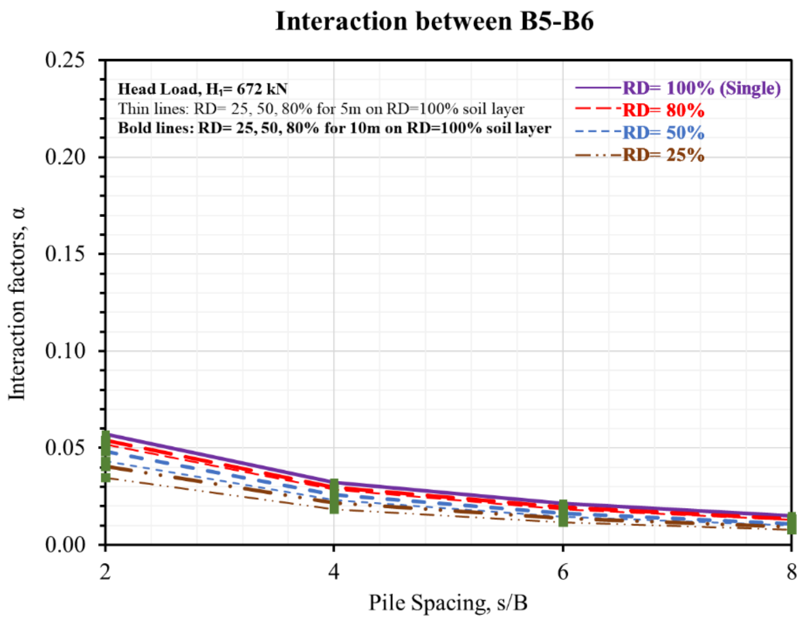

Figure A1.15 The interaction factors in between source pile B5 and receiver pile B6 in Case-1d, Head load on source pile: 672 kN, For two-layer model relative densities of the upper layer, varies 25%, 50%, %80. For single-layer model RD=100%.

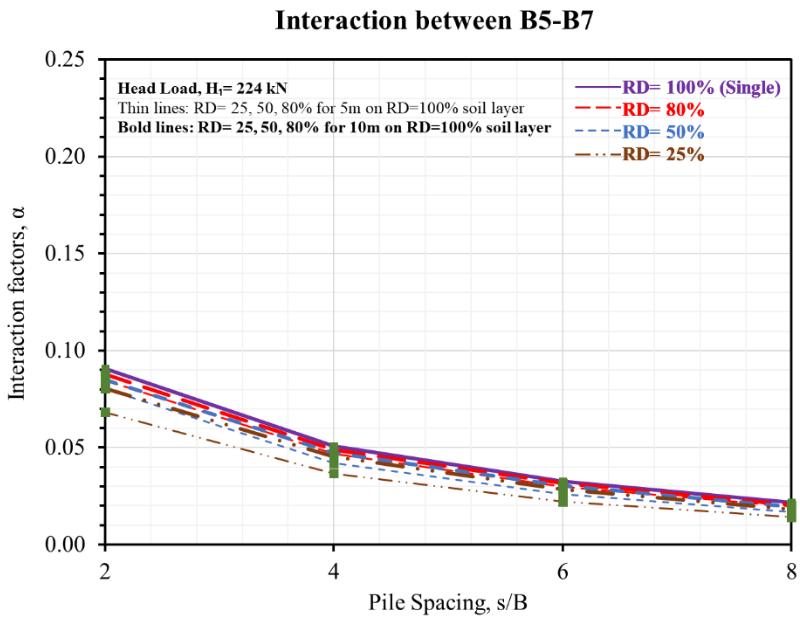

Figure A1.16 The interaction factors in between source pile B5 and receiver pile B7 in Case-1d, Head load on source pile: 224 kN, For two-layer model relative densities of the upper layer, varies 25%, 50%, %80. For single-layer model RD=100%.

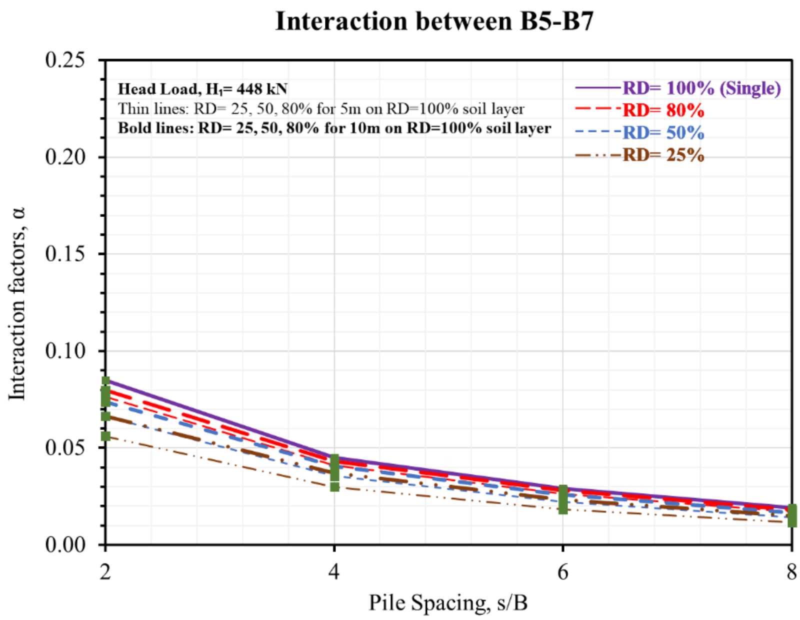

Figure A1.17 The interaction factors in between source pile B5 and receiver pile B7 in Case-1d, Head load on source pile: 448 kN, For two-layer model relative densities of the upper layer, varies 25%, 50%, %80. For single-layer model RD=100%.

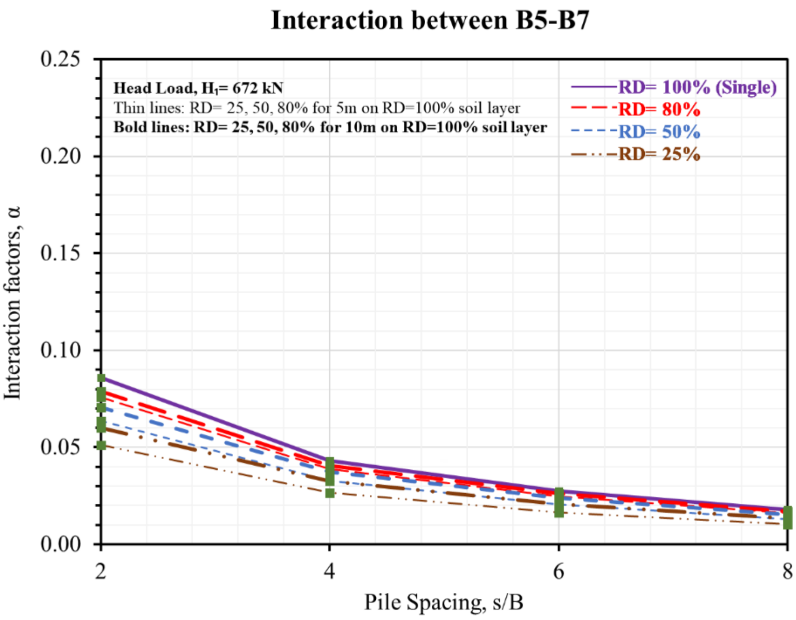

Figure A1.18 The interaction factors in between source pile B5 and receiver pile B7 in Case-1d, Head load on source pile: 672 kN, For two-layer model relative densities of the upper layer, varies 25%, 50%, %80. For single-layer model RD=100%.

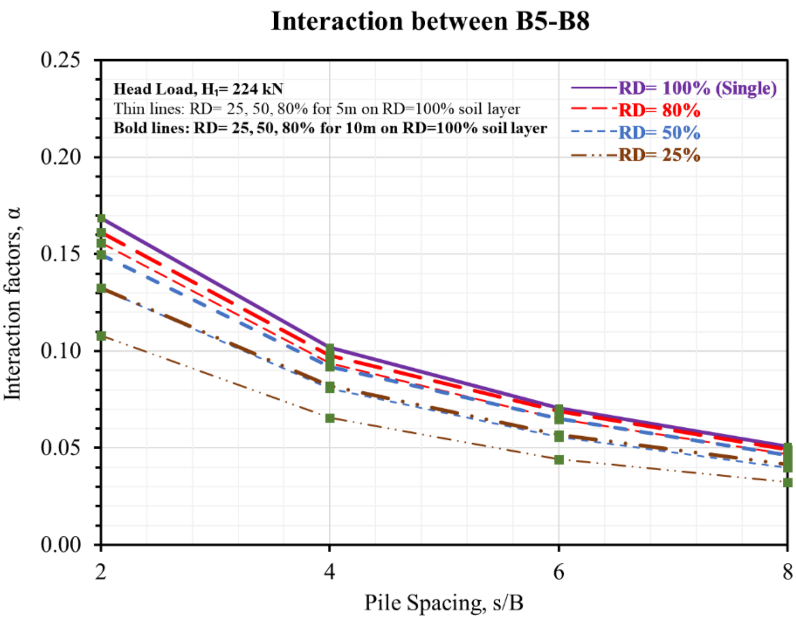

Figure A1.19 The interaction factors in between source pile B5 and receiver pile B8 in Case-1d, Head load on source pile: 224 kN, For two-layer model relative densities of the upper layer, varies 25%, 50%, %80. For single-layer model RD=100%.

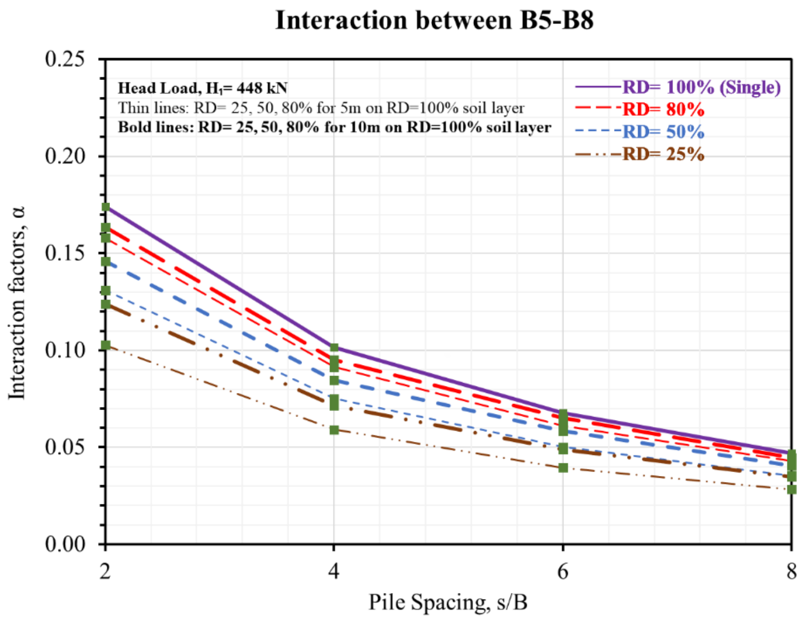

Figure A1.20 The interaction factors in between source pile B5 and receiver pile B8 in Case-1d, Head load on source pile: 448 kN, For two-layer model relative densities of the upper layer, varies 25%, 50%, %80. For single-layer model RD=100%.

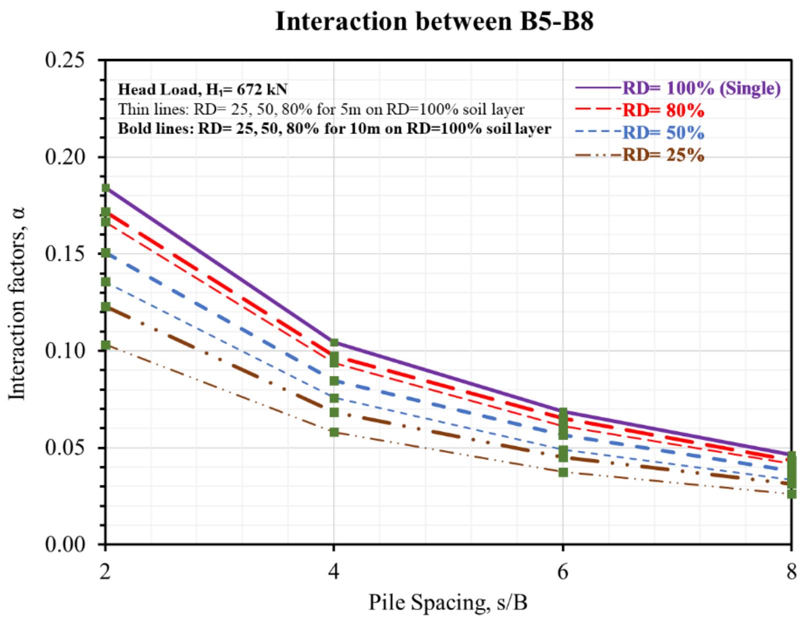

Figure A1.21 The interaction factors in between source pile B5 and receiver pile B8 in Case-1d, Head load on source pile: 672 kN, For two-layer model relative densities of the upper layer, varies 25%, 50%, %80. For single-layer model RD=100%.

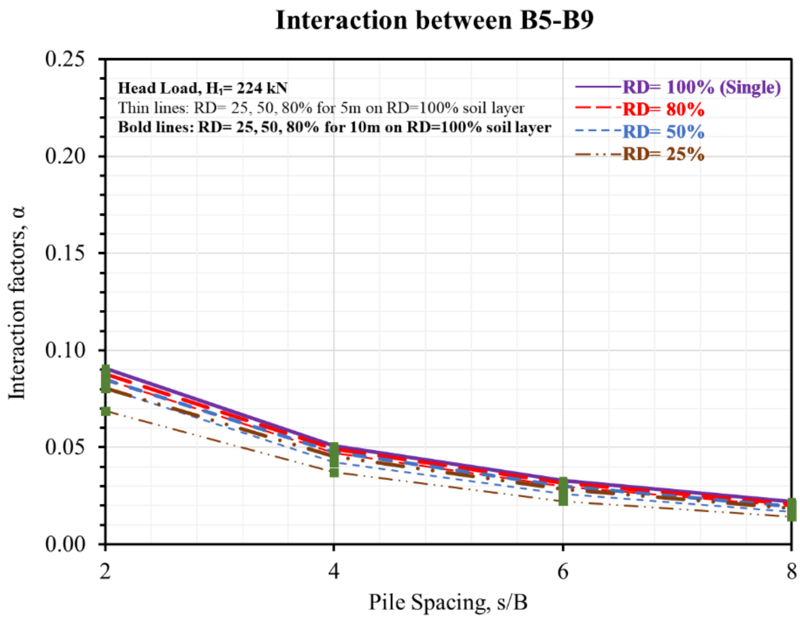

Figure A1.22 The interaction factors in between source pile B5 and receiver pile B9 in Case-1d, Head load on source pile: 224 kN, For two-layer model relative densities of the upper layer, varies 25%, 50%, %80. For single-layer model RD=100%.

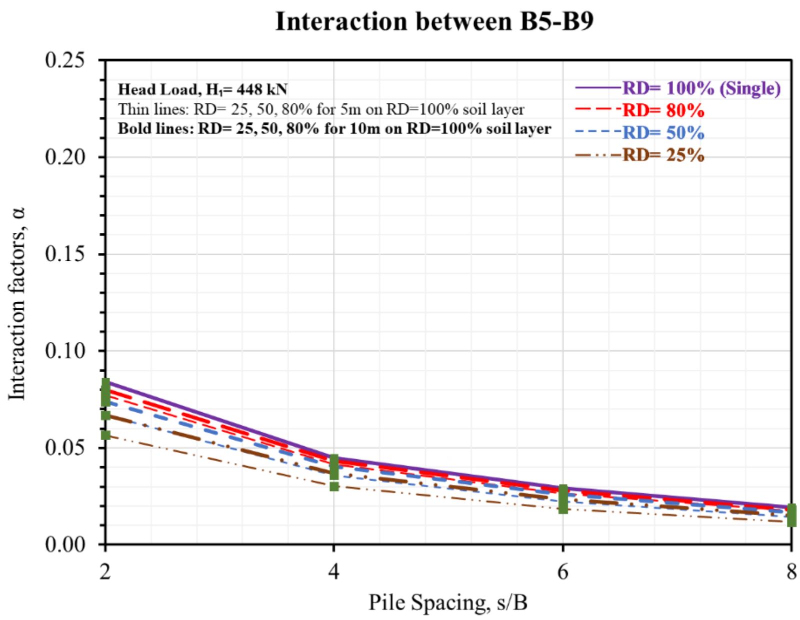

Figure A1.23 The interaction factors in between source pile B5 and receiver pile B9 in Case-1d, Head load on source pile: 448 kN, For two-layer model relative densities of the upper layer, varies 25%, 50%, %80. For single-layer model RD=100%.

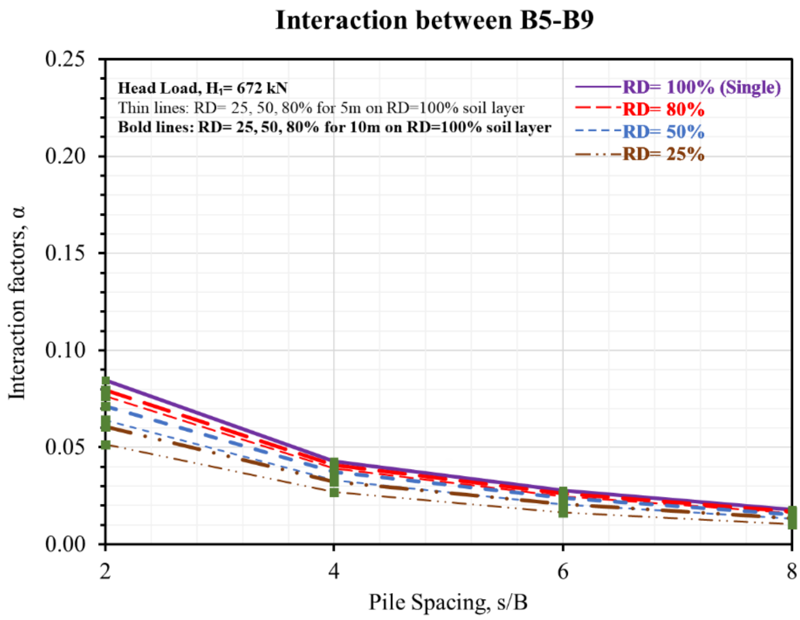

Figure A1.24 The interaction factors in between source pile B5 and receiver pile B9 in Case-1d, Head load on source pile: 672 kN, For two-layer model relative densities of the upper layer, varies 25%, 50%, %80. For single-layer model RD=100%.

Appendix-2 The analyses result of Case-2d shows the interaction factor between source pile and receiver piles.

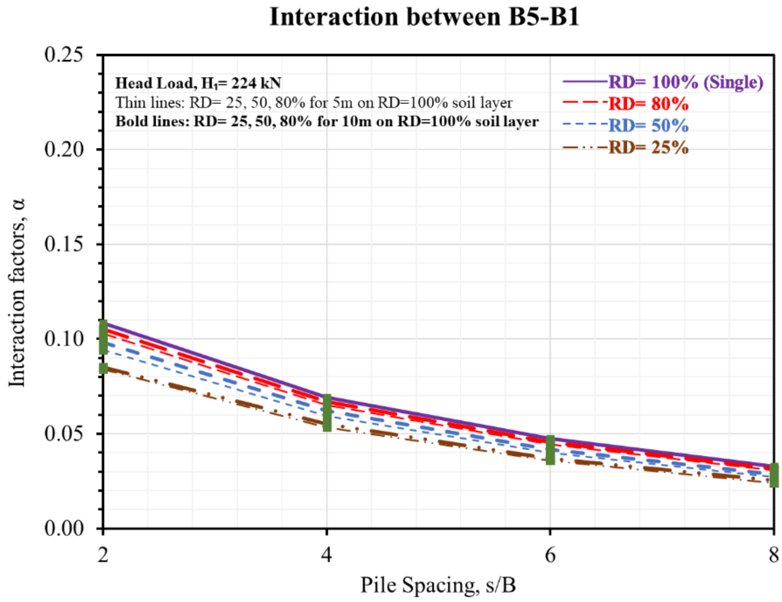

Figure B1.1 The interaction factors in between source pile B5 and receiver pile B1 in Case-2d, Head load on source pile: 224 kN, For two-layer model relative densities of the upper layer, varies 25%, 50%, %80. For single-layer model RD=100%.

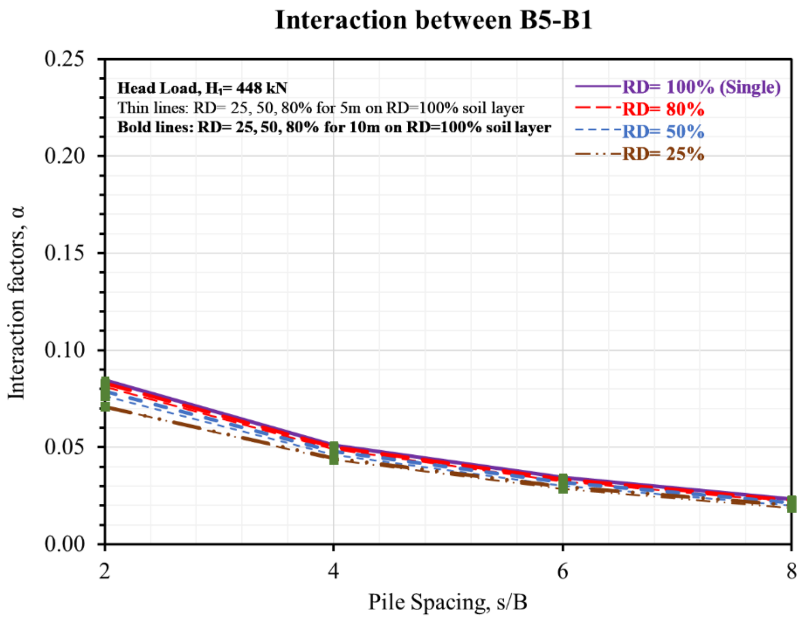

Figure B1.2 The interaction factors in between source pile B5 and receiver pile B1 in Case-2d, Head load on source pile: 448 kN, For two-layer model relative densities of the upper layer, varies 25%, 50%, %80. For single-layer model RD=100%.

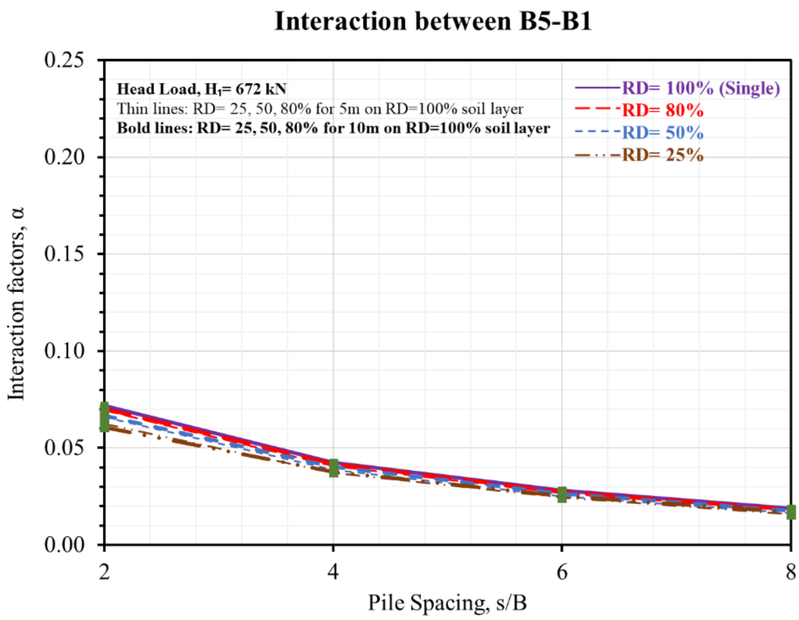

Figure B1.3 The interaction factors in between source pile B5 and receiver pile B1 in Case-2d, Head load on source pile: 672 kN, For two-layer model relative densities of the upper layer, varies 25%, 50%, %80. For single-layer model RD=100%.

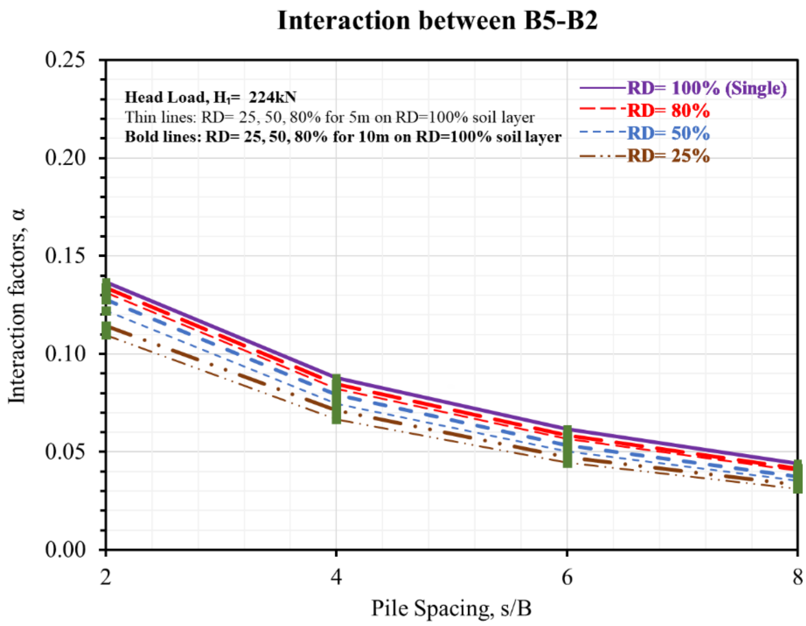

Figure B1.4 The interaction factors in between source pile B5 and receiver pile B2 in Case-2d, Head load on source pile: 224 kN, For two-layer model relative densities of the upper layer, varies 25%, 50%, %80. For single-layer model RD=100%.

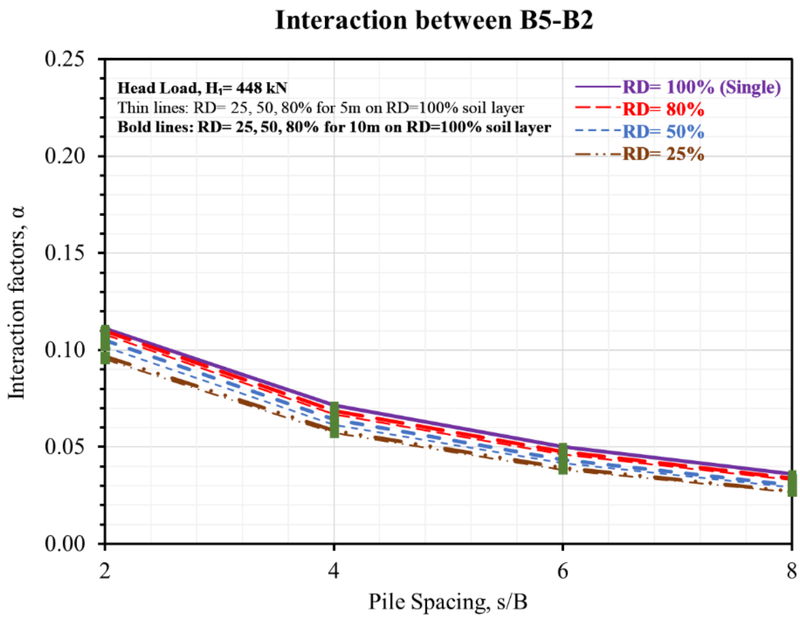

Figure B1.5 The interaction factors in between source pile B5 and receiver pile B2 in Case-2d, Head load on source pile: 448 kN, For two-layer model relative densities of the upper layer, varies 25%, 50%, %80. For single-layer model RD=100%.

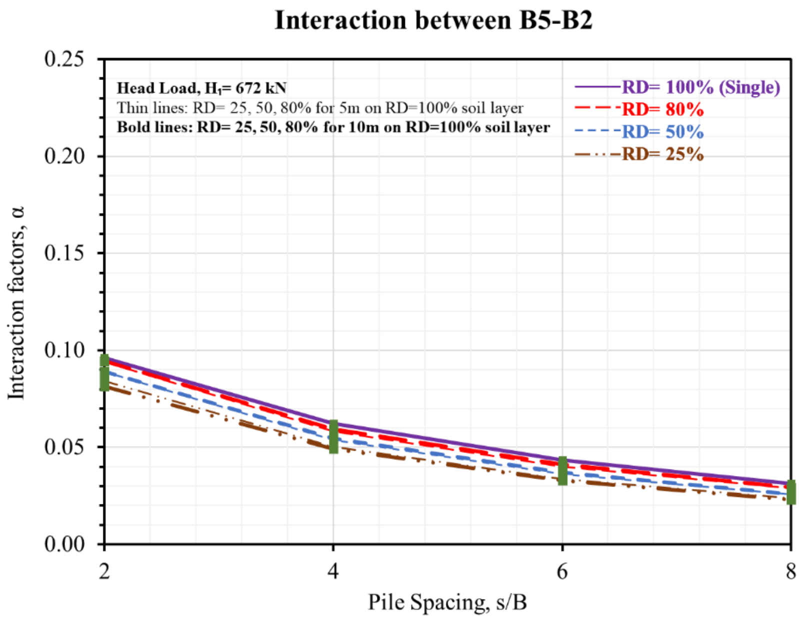

Figure B1.6 The interaction factors in between source pile B5 and receiver pile B2 in Case-2d, Head load on source pile: 672 kN, For two-layer model relative densities of the upper layer, varies 25%, 50%, %80. For single-layer model RD=100%.

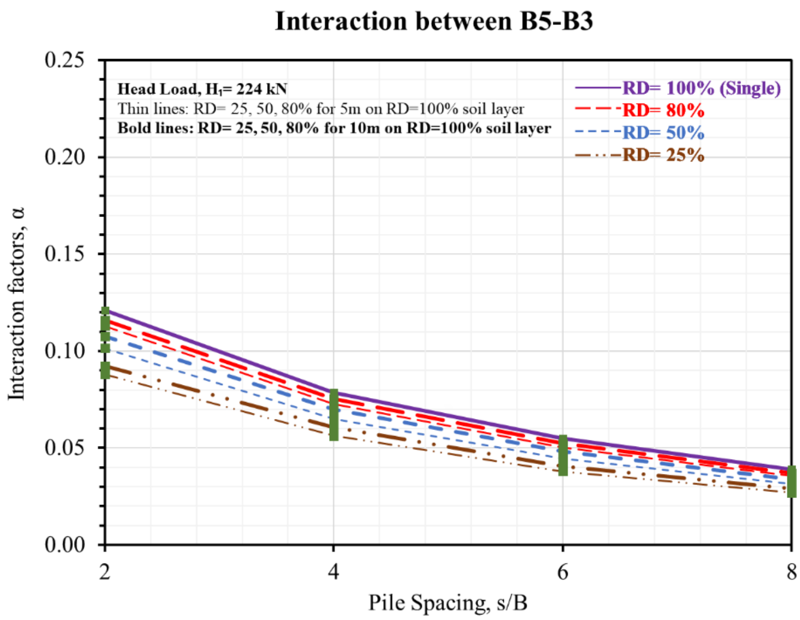

Figure B1.7 The interaction factors in between source pile B5 and receiver pile B3 in Case-2d, Head load on source pile: 224 kN, For two-layer model relative densities of the upper layer, varies 25%, 50%, %80. For single-layer model RD=100%.

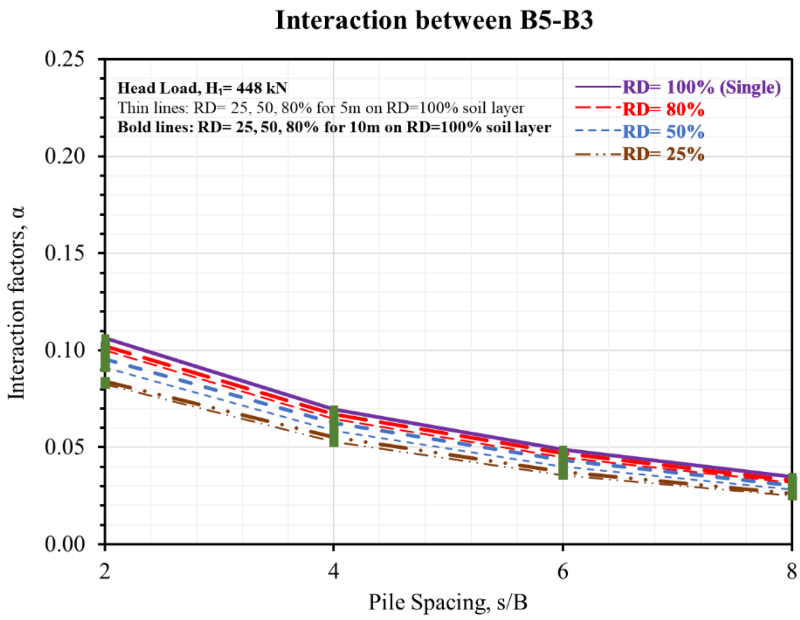

Figure B1.8 The interaction factors in between source pile B5 and receiver pile B3 in Case-2d, Head load on source pile: 448 kN, For two-layer model relative densities of the upper layer, varies 25%, 50%, %80. For single-layer model RD=100%.

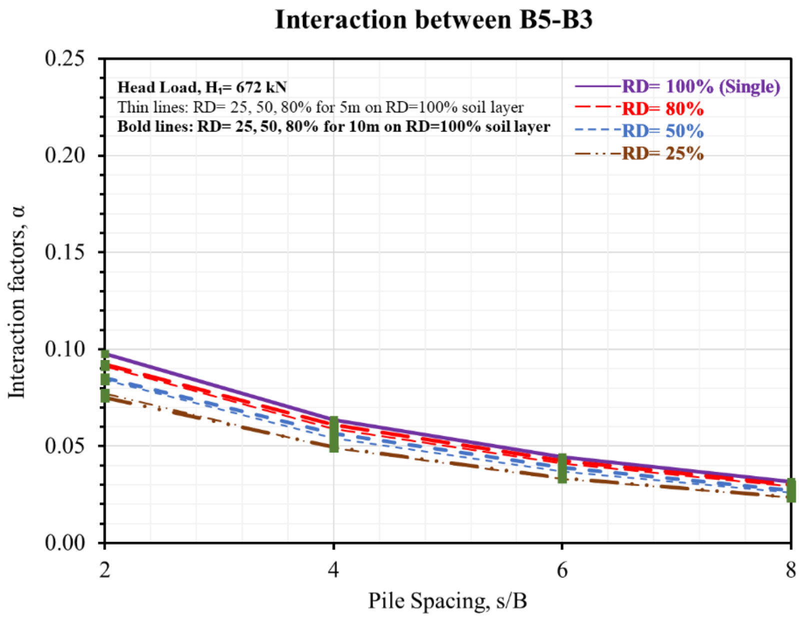

Figure B1.9 The interaction factors in between source pile B5 and receiver pile B3 in Case-2d, Head load on source pile: 672 kN, For two-layer model relative densities of the upper layer, varies 25%, 50%, %80. For single-layer model RD=100%.

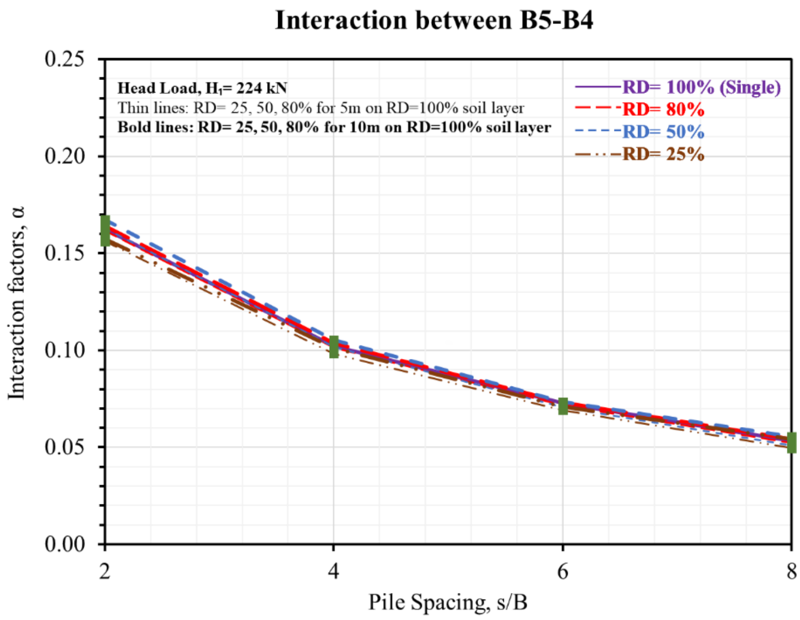

Figure B1.10 The interaction factors in between source pile B5 and receiver pile B4 in Case-2d, Head load on source pile: 224 kN, For two-layer model relative densities of the upper layer, varies 25%, 50%, %80. For single-layer model RD=100%.

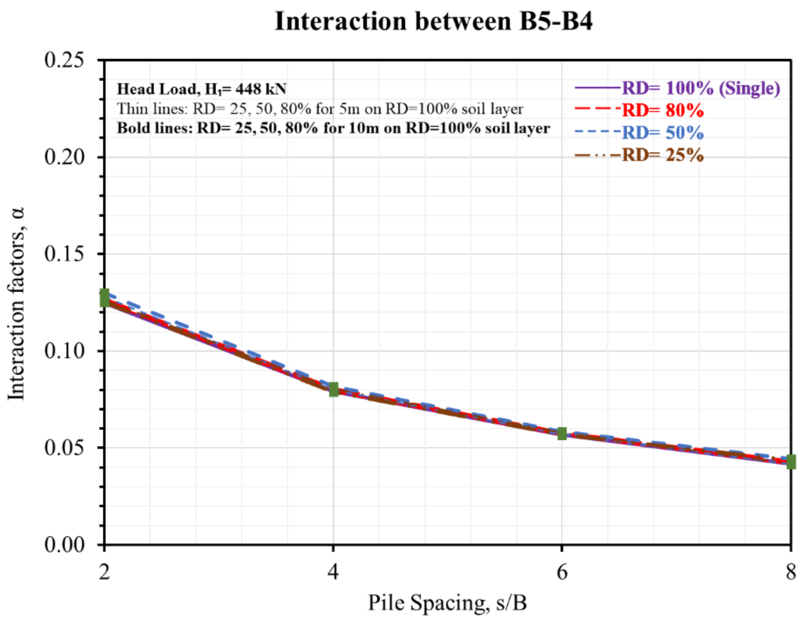

Figure B1.11 The interaction factors in between source pile B5 and receiver pile B4 in Case-2d, Head load on source pile: 448 kN, For two-layer model relative densities of the upper layer, varies 25%, 50%, %80. For single-layer model RD=100%.

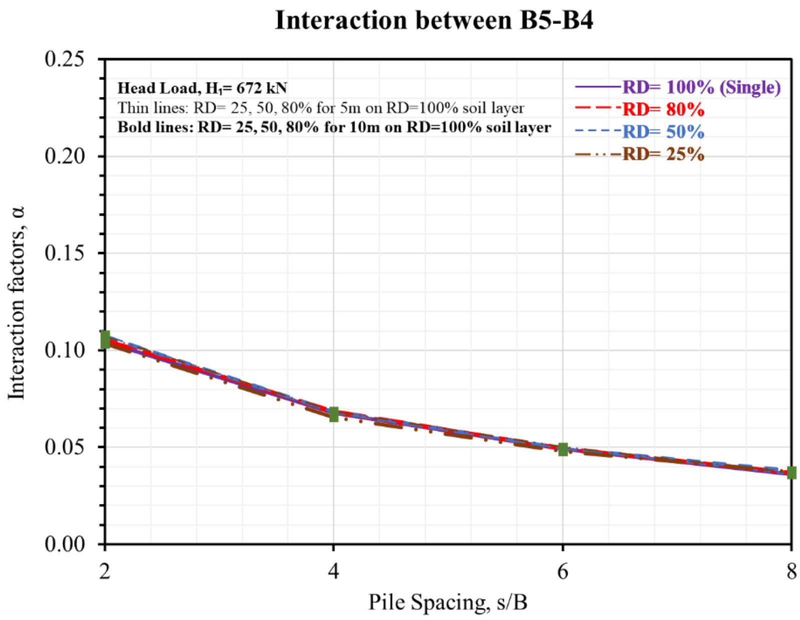

Figure B1.12 The interaction factors in between source pile B5 and receiver pile B4 in Case-2d, Head load on source pile: 672 kN, For two-layer model relative densities of the upper layer, varies 25%, 50%, %80. For single-layer model RD=100%.

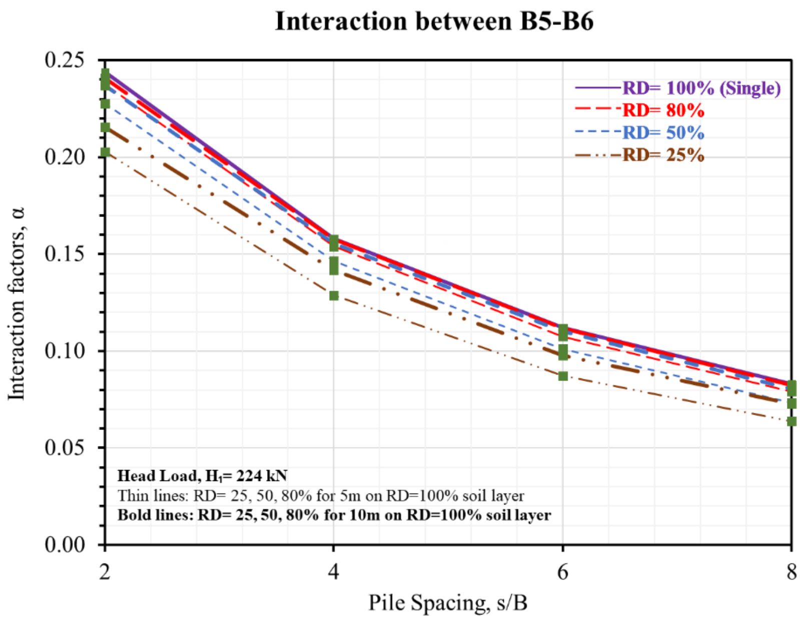

Figure B1.13 The interaction factors in between source pile B5 and receiver pile B6 in Case-2d, Head load on source pile: 224 kN, For two-layer model relative densities of the upper layer, varies 25%, 50%, %80. For single-layer model RD=100%.

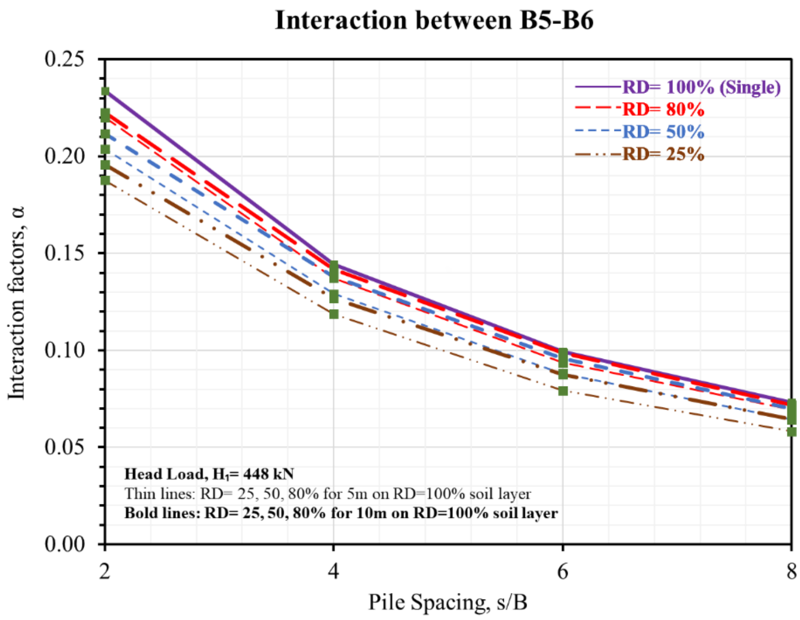

Figure B1.14 The interaction factors in between source pile B5 and receiver pile B6 in Case-2d, Head load on source pile: 448 kN, For two-layer model relative densities of the upper layer, varies 25%, 50%, %80. For single-layer model RD=100%.

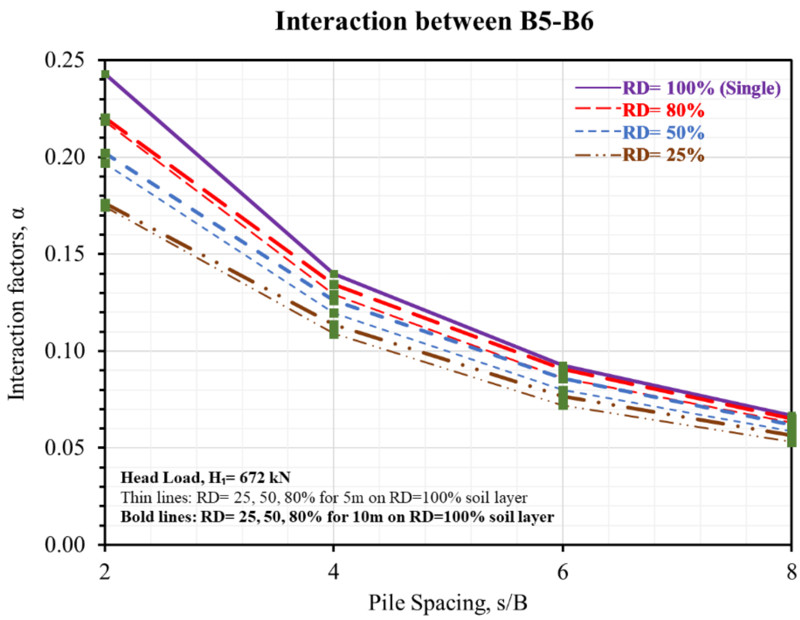

Figure B1.15 The interaction factors in between source pile B5 and receiver pile B6 in Case-2d, Head load on source pile: 672 kN, For two-layer model relative densities of the upper layer, varies 25%, 50%, %80. For single-layer model RD=100%.

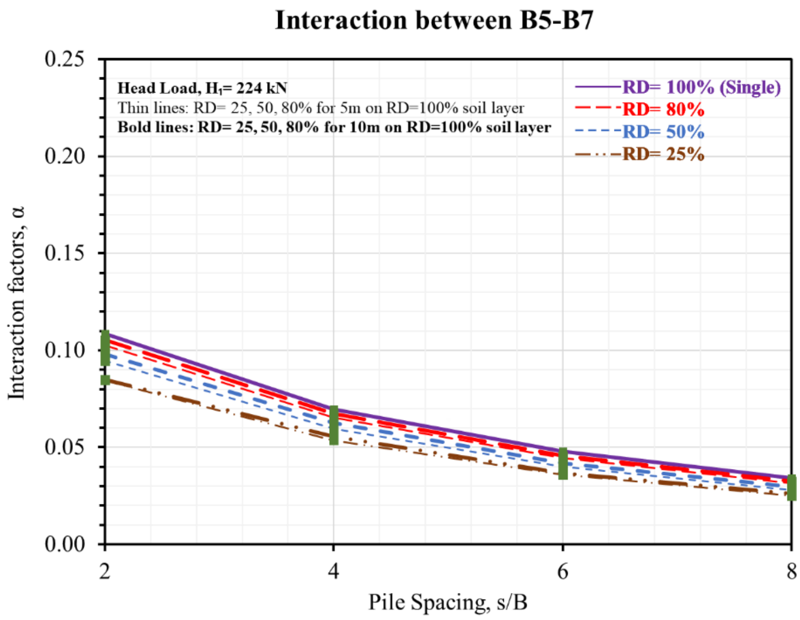

Figure B1.16 The interaction factors in between source pile B5 and receiver pile B7 in Case-2d, Head load on source pile: 224 kN, For two-layer model relative densities of the upper layer, varies 25%, 50%, %80. For single-layer model RD=100%.

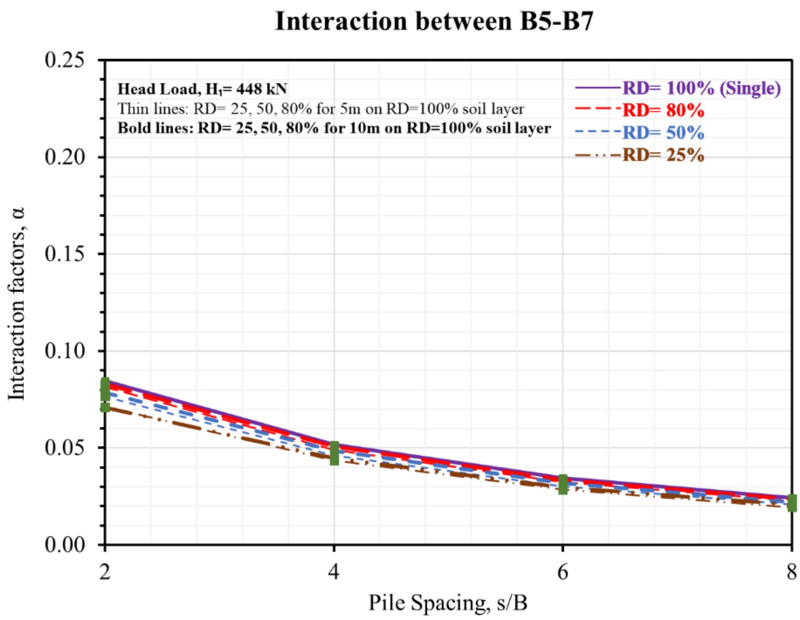

Figure B1.17 The interaction factors in between source pile B5 and receiver pile B7 in Case-2d, Head load on source pile: 448 kN, For two-layer model relative densities of the upper layer, varies 25%, 50%, %80. For single-layer model RD=100%.

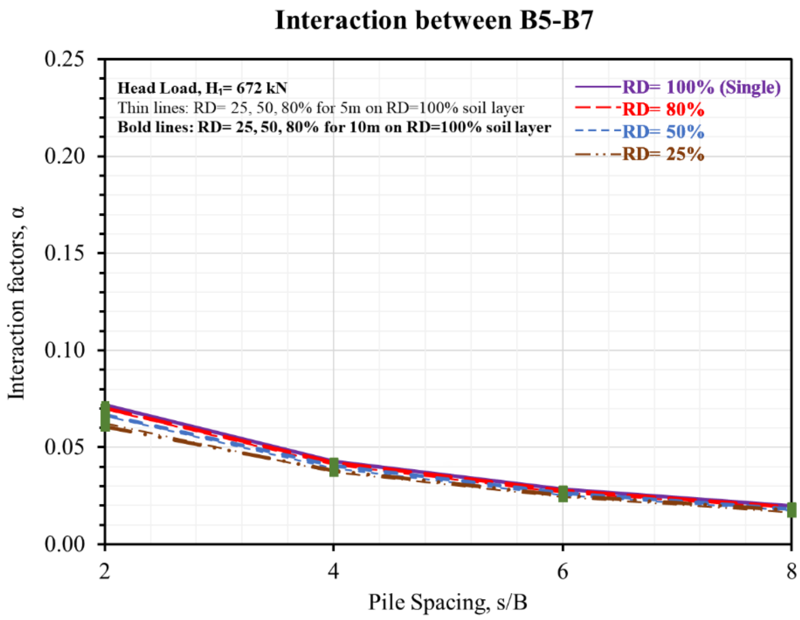

Figure B1.18 The interaction factors in between source pile B5 and receiver pile B7 in Case-2d, Head load on source pile: 672 kN, For two-layer model relative densities of the upper layer, varies 25%, 50%, %80. For single-layer model RD=100%.

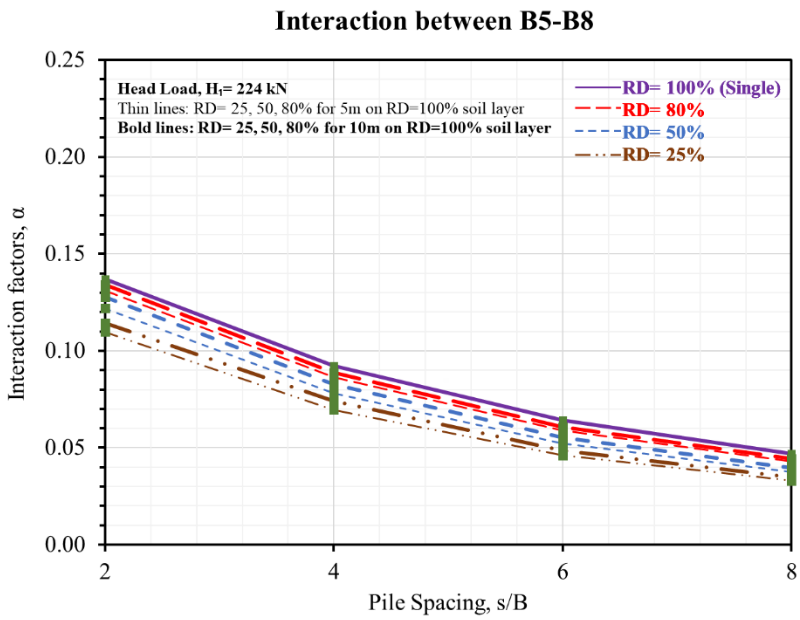

Figure B1.19 The interaction factors in between source pile B5 and receiver pile B8 in Case-2d, Head load on source pile: 224 kN, For two-layer model relative densities of the upper layer, varies 25%, 50%, %80. For single-layer model RD=100%.

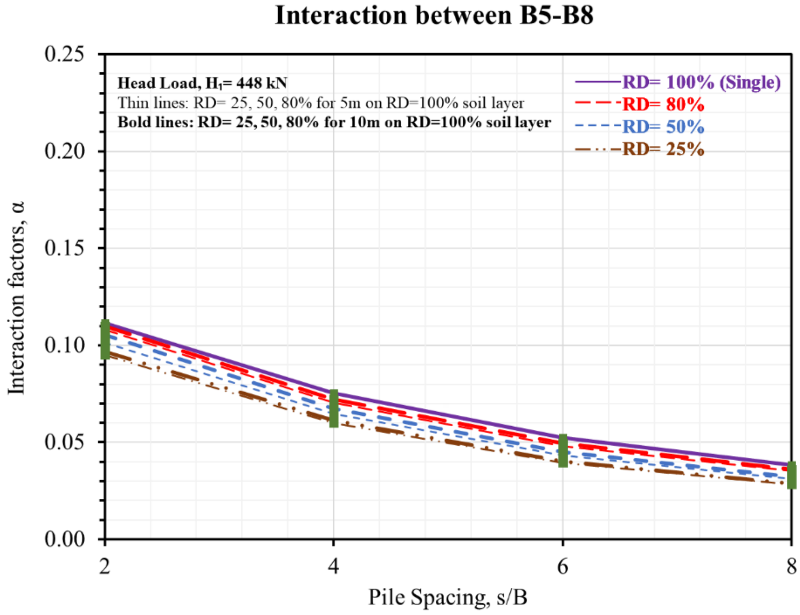

Figure B1.20 The interaction factors in between source pile B5 and receiver pile B8 in Case-2d, Head load on source pile: 448 kN, For two-layer model relative densities of the upper layer, varies 25%, 50%, %80. For single-layer model RD=100%.

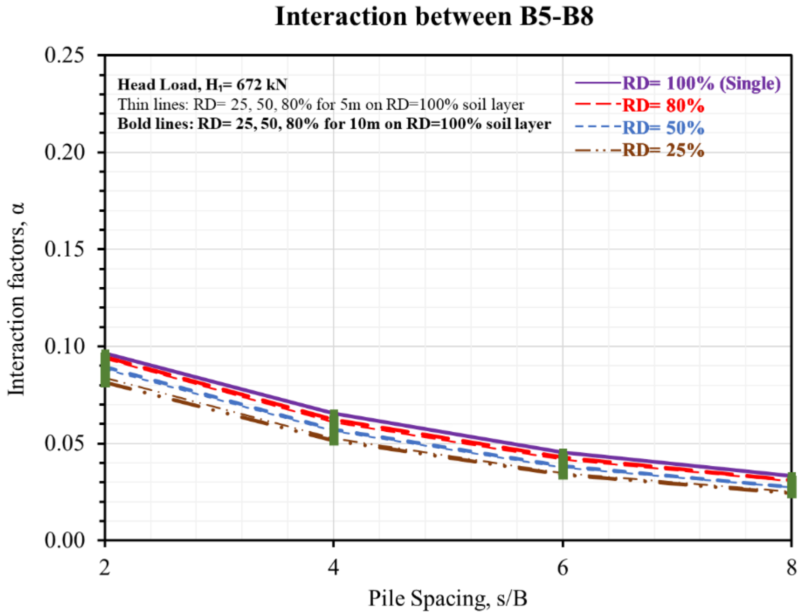

Figure B1.21 The interaction factors in between source pile B5 and receiver pile B8 in Case-2d, Head load on source pile: 672 kN, For two-layer model relative densities of the upper layer, varies 25%, 50%, %80. For single-layer model RD=100%.

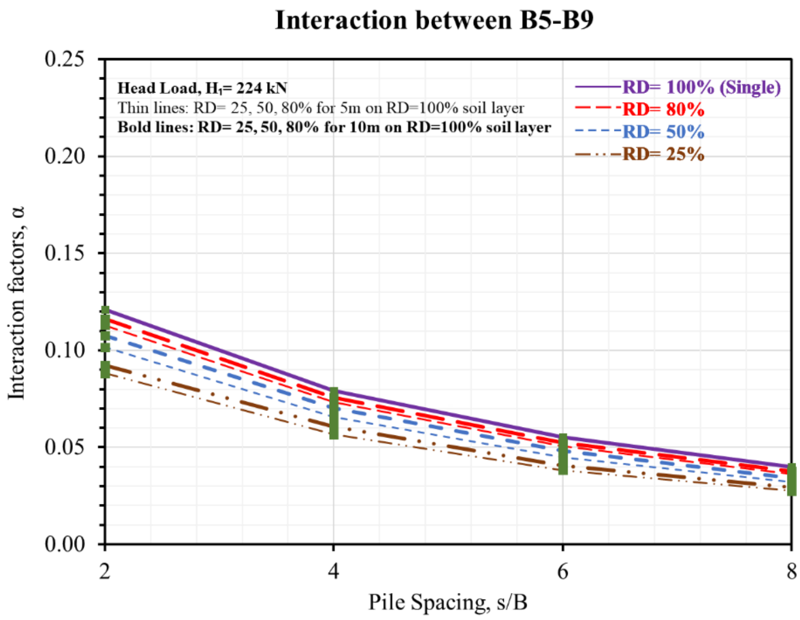

Figure B1.22 The interaction factors in between source pile B5 and receiver pile B9 in Case-2d, Head load on source pile: 224 kN, For two-layer model relative densities of the upper layer, varies 25%, 50%, %80. For single-layer model RD=100%.

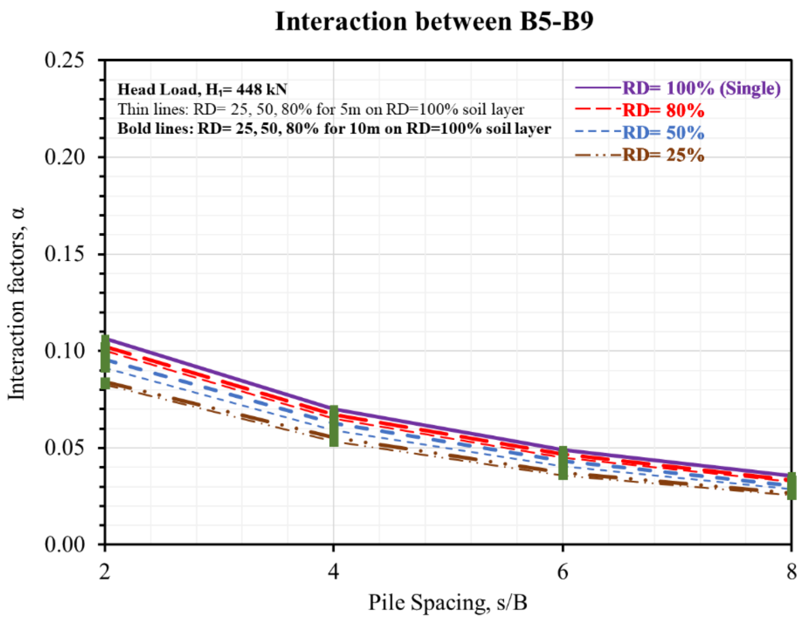

Figure B1.23 The interaction factors in between source pile B5 and receiver pile B9 in Case-2d, Head load on source pile: 448 kN, For two-layer model relative densities of the upper layer, varies 25%, 50%, %80. For single-layer model RD=100%.

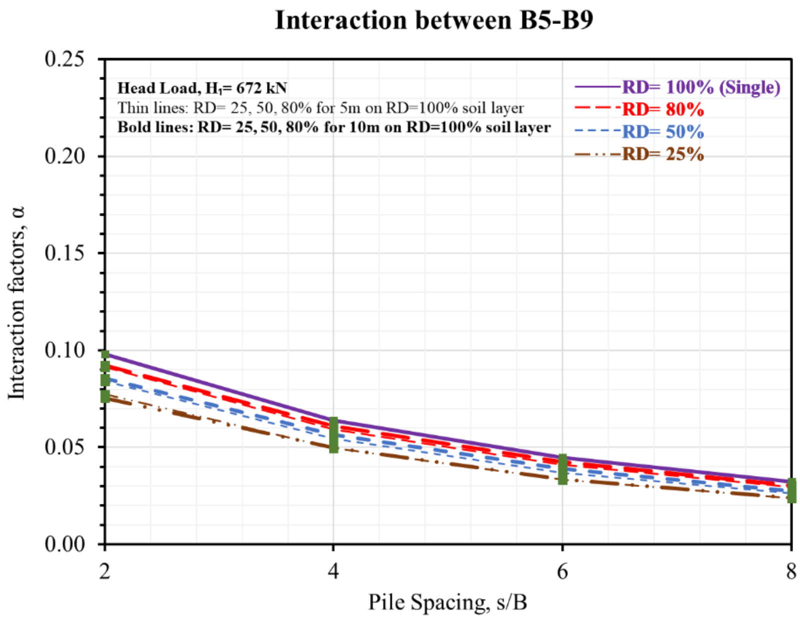

Figure B1.24 The interaction factors in between source pile B5 and receiver pile B9 in Case-2d, Head load on source pile: 672 kN, For two-layer model relative densities of the upper layer, varies 25%, 50%, %80. For single-layer model RD=100%.